

Energy Harvesting for Wireless IoT Use Cases: A Generic Feasibility Model and Tradeoff Study

Dries Van Leemput^{ID}, Adnan Sabovic^{ID}, Khodr Hammoud^{ID}, *Graduate Student Member, IEEE*, Jeroen Famaey^{ID}, *Senior Member, IEEE*, Sofie Pollin^{ID}, *Senior Member, IEEE*, and Eli De Poorter^{ID}

Abstract—A batteryless Internet of Things (IoT) offers a sustainable alternative to battery-powered IoT devices, which produce billions of dead batteries every year. Devices are instead powered by a small supercapacitor, which is recharged by a renewable energy source. However, since IoT devices are often characterized by intermittent periods of high energy consumption followed by periods of reduced activity, conventional average energy consumption models cannot be used to assess if IoT devices can be powered by energy harvesters. Therefore, this article presents an alternative feasibility evaluation approach that focuses on modeling the worst case periods with peak energy consumption and short idle times, which pose the highest constraints on the capacitor's behavior. This approach simplifies the characterization of the wireless technology energy consumption as these worst case periods can be determined by a few parameters. The methodology is then applied to combinations of popular IoT technologies (LoRaWAN, BLE Mesh, and 6TiSCH) and energy sources (solar, kinetic, and radio frequency energy) for two common IoT use cases. We show that the proposed parameters can be successfully extracted with power measurements for different network configurations and that the Power Management Unit configuration has a nonnegligible impact on the communication requirements. Finally, we discuss how to apply the model to other technologies and other use cases.

Index Terms—6TiSCH, Bluetooth low energy (BLE), energy harvesting, feasibility study, Internet of Things (IoT), long range wide area network (LoRaWAN).

I. INTRODUCTION

THE Internet of Things (IoT) enables the connection of billions of devices to the Internet and perform sensing, actuating, communication, and localization operations. Due to their relatively low power consumption and because of the desired use cases, these devices are often battery-powered. However, batteries are hazardous, bulky, expensive,

Manuscript received 7 September 2022; revised 6 January 2023 and 22 February 2023; accepted 24 March 2023. Date of publication 31 March 2023; date of current version 24 August 2023. This work was supported by the Flemish FWO SBO through the Sustainable Internet of Batteryless Things Project under Grant S001521N IoBaLeT. (*Corresponding author: Dries Van Leemput*.)

Dries Van Leemput and Eli De Poorter are with the IDLab, Department of Information Technology, Ghent University-imec, 9000 Ghent, Belgium (e-mail: dries.vanleemput@ugent.be; eli.depoorter@ugent.be).

Adnan Sabovic and Jeroen Famaey are with the IDLab, Department of Computer Science, University of Antwerp-imec, 2000 Antwerpen, Belgium (e-mail: adnan.sabovic@uantwerpen.be; jeroen.famaey@uantwerpen.be).

Khodr Hammoud and Sofie Pollin are with the ESAT-WaveCoRE, Department of Electrical Engineering, KU Leuven, 3001 Heverlee, Belgium (e-mail: khodr.hammoud@kuleuven.be; sofie.pollin@kuleuven.be).

Digital Object Identifier 10.1109/JIOT.2023.3263543

sensitive to temperature changes, and last at most a few years, even when rechargeable. Therefore, disposing of billions of dead batteries per year is both economically and ecologically unacceptable [1]. In addition, some use cases require devices to be deployed in remote or hard-to-reach environments, which makes the replacement of batteries expensive and dangerous, if not impossible. Therefore, there has been a significant recent interest in developing batteryless and perpetual IoT devices by using energy harvesting techniques. These devices generally consist of a microcontroller unit (MCU), radio chip, one or more sensors or actuators, power management unit (PMU), and a supercapacitor. The PMU charges the capacitor using an energy source, which can be solar, kinetic, thermal, radio frequency (RF) energy, etc. As the energy source harvests energy from its environment, the type of energy source is highly dependent on this environment.

However, IoT devices are used for a wide range of use cases: transport systems, hazardous environment sensing, healthcare, smart meters, asset tracking, infrastructure monitoring, etc. Each of these use cases has different requirements and entails various deployment environments, which in turn provide varying opportunities to harvest energy. Additionally, plenty of wireless technologies offer IoT connectivity with divergent communication capabilities. Therefore, the correct choice of wireless technology and energy source for a specific use case might prove to be difficult and the wrong choice could result in a waste of time and resources. It is, therefore, essential to know which combinations of wireless technologies and energy sources are feasible for a particular use and to identify the boundaries of the use case requirements for these combinations. Although a comparison of the average power consumption of the wireless technology and harvested power by the energy source allows for an initial sense of the feasibility, it does not take the nature of IoT use cases and wireless technologies into account, nor does it consider the (dis)charge behavior of a capacitor. IoT devices usually reside most of the time in a sleep state and wake up to perform a task, resulting in a current peak. Due to their sparse energy density compared to batteries, supercapacitors are able to supply a limited amount of energy during current peaks but need to be recharged during idle periods. Therefore, the scheduling of these current peaks has a major influence on the feasibility of the system. However, it is often impossible to characterize the entire operation of a wireless technology and evaluate the capacitor's behavior for the complete operational lifetime.

TABLE I
COMPARISON OF RELATED WORKS TO OUR WORK

Work	Wireless technology					Energy source			Storage element		Use Cases	
	LoRaWAN	BLE	6TiSCH	NB-IoT	SigFox	Solar	Kinetic	RF	Thermal	Capacitor	Battery	
[3]	✓	✗	✗	✗	✗	✓	✗	✓	✓	✗	✓	Industry 4.0
[4]	✓	✗	✗	✗	✗	✓	✗	✗	✗	✓	✓	Env. monitoring
[5], [6]	✓	✗	✗	✗	✗	✗	✗	✗	✗	✓	✗	-
[7]	✓	✗	✗	✗	✗	✗	✗	✗	✗	✓	✗	Env. monitoring
[8]	✓	✗	✗	✗	✗	✗	✗	✓	✗	✓	✗	-
[9]	✗	✓	✗	✗	✗	✗	✗	✓	✗	✗	✗	Env. monitoring
[10]	✗	✓	✗	✗	✗	✗	✗	✗	✗	✓	✗	Logistics
[11]	✗	✗	✓	✗	✗	✓	✗	✗	✗	✗	✓	-
[12]	✗	✗	✓	✗	✗	✗	✓	✗	✗	✗	✓	Manufacturing, railway transport
[13]	✗	✗	✓	✗	✗	✗	✓	✗	✗	✓	✗	Industry 4.0
[16]	✓	✓	✗	✓	✓	✗	✓	✗	✗	✗	✓	Horse monitoring
[17]	✓	✓	✗	✓	✓	✓	✗	✗	✗	✓	✗	-
[18]	✓	✓	✗	✓	✓	✓	✗	✓	✗	✗	✗	Smart metering
Our work	✓	✓	✓	✗	✗	✓	✓	✓	✗	✓	✗	Asset tracking, building automation

To that end, this article presents a generic model to analyze the feasibility of energy harvesting for IoT use cases, which considers the nature of these use cases, wireless technologies, and the (dis)charge behavior of capacitors. To avoid a complete characterization of the wireless technology, we propose three well-chosen parameters that specify the worst case scheduling period for the (dis)charge behavior of the capacitor. As a result, it suffices to only evaluate this worst case scheduling period, as other moments impose more lenient requirements on the capacitor. Furthermore, due to abstracting the operation of the wireless technology by three parameters that specify the worst cast scheduling period, any technology can be quickly evaluated. These parameters can be obtained by examining the wireless technology for a certain configuration, through simulations, power measurements, standard specifications, data sheets, etc. As an example, we apply the model to three popular wireless technologies: 1) long range wide area network (LoRaWAN); 2) Bluetooth low energy (BLE) Mesh; and 3) 6TiSCH using three common energy sources: 1) solar; 2) kinetic; and 3) RF energy. This allows for a feasibility study of two of the most prominent IoT use cases: long-range asset tracking and dense building automation, for different combinations of the aforementioned wireless technologies and energy sources. These were selected based on market studies and a preliminary study featuring 21 companies involved in IoT.

In summary, the main contributions of this article are as follows.

- 1) A generic feasibility model to analyze the feasibility of energy harvesting for IoT use cases, considering different combinations of wireless technologies and energy sources. The model takes the nature of IoT use cases and wireless technologies into account, and their impact on the (dis)charge behavior of supercapacitors. By identifying the worst case scheduling period, a complete characterization of the wireless technology is not required, facilitating the evaluation of any technology. The Python code of the model is available as open-source code

online and can be extended to include additional energy sources, wireless technologies, and IoT use cases [2].

- 2) Characterization of the worst case energy consumption period in terms of energy harvesting for three commonly used wireless technologies (LoRaWAN, BLE Mesh, and 6TiSCH). This is in contrast to already existing energy models, which calculate the average energy consumption.
- 3) Feasibility and tradeoff analysis of two prominent IoT use cases (long-range asset tracking and dense building automation) for a combination of the selected wireless technologies and energy sources to identify promising combinations for future research.

The remainder of this article is structured as follows. First, Section II presents an overview of related work on the feasibility of energy harvesting for IoT. Next, Section III describes the results of the preliminary industry study to select the evaluated wireless technologies, energy sources, and IoT use cases. The details of the worst case energy consumption model are explained in Section IV, including the necessary assumptions to employ the model. Next, Section V lists some typical values of the harvested power for the selected energy sources, and Section VI characterizes the necessary energy parameters and boundaries of the wireless technologies. The results of these sections are then used in Section VII to perform a feasibility and tradeoff analysis and suggestions are presented to extend the model toward other use cases. Finally, Section VIII ends this article with a conclusion.

II. RELATED WORK

Table I gives an overview of existing literature on the feasibility of energy harvesting for wireless sensor networks (WSNs). For each work, the considered wireless technology, energy source, energy storage type, and evaluated use cases are indicated. While other works include alternative wireless technologies or energy sources, we highlight the most widely

used and focus on the ones examined in this article to evaluate the differences and analogies to our work.

The feasibility of energy harvesting for LoRaWAN networks has been studied extensively in the literature. Sherazi et al. [3] presented a model to evaluate the lifetime of battery-powered LoRaWAN nodes and the possibility of using renewable energy sources to feed the nodes in industrial environments. The authors consider a combination of indoor light, thermoelectric, and RF energy sources. Mabon et al. [4] proposed a generic optimization methodology to dimension the energy storage elements of an autonomous node and perform an experimental validation on a LoRaWAN platform. They assume a supercapacitor in combination with a battery, which provides power during periods without light harvesting. Delgado et al. present a batteryless LoRaWAN device model, including a supercapacitor, a voltage source, and variable load resistance in [5]. They evaluate the required capacitor and minimum voltage, and the impact of the turn-on threshold on the reliability. The authors extend their model in [6] with a current source and nonideal supercapacitor. In addition, they present a Markov model to characterize the performance of a LoRaWAN Class A device and evaluate the capacitor size, feasible transmission interval, and optimal turn-on threshold assuming a continuous harvesting power. Sabovic et al. [7] defined an optimization problem to determine the optimal supercapacitor voltage to perform and schedule application tasks, using the model presented in [5]. They measure the execution time and energy consumption of a LoRaWAN device for constant harvesting power. Finally, Finnegan et al. [8] explored the boundaries of powering a LoRaWAN device with ambient RF energy sources, using an analytical LoRaWAN device model and RF energy data found in the literature. The authors estimate the capacitance for multiple data rates and analyze the impact of leakage current, sleep current, and PMU efficiency on the required harvesting power.

Energy harvesting for BLE networks is studied in [9]. Relevant technologies in RF energy harvesting mechanisms are discussed and an investigation of RF energy harvesting using two proof-of-concept systems is performed, of which one employs BLE advertising messages. The authors point out the impact of the distance to the energy source, the amount of transferred data, and the leakage current of supercapacitors. Sultania et al. [10] proposed an analytical model for the performance of a batteryless BLE Mesh low-power node (LPN) as a function of downlink latency and reliability. They measure the energy consumption and execution time of a BLE Mesh LPN and analyze different capacitor sizes and continuous harvested power values for network-specific parameters, including friend queue size, receive delay, and packet size.

Xhafa et al. [11] investigated the possibility of powering nodes in a time-slotted channel hopping (TSCH) network with solar energy. They compare the average consumed power with the average harvested power for both the default and an enhanced TSCH layer and conclude that both options draw more power than a solar panel can provide. To that end, Das et al. [12] proposed a hierarchical network management scheme and an asynchronous communication scheme to include energy-harvesting devices in TSCH networks using

mechanical vibration energy. The authors evaluate the solutions in terms of management efficiency and energy consumption, and show that they are feasible for an automotive manufacturing and railway transport use case. Chew et al. [13] focused on the TSCH joining process and present a duty-cycle joining process that enables batteryless nodes to join the network with less energy wastage. They show that a capacitor can be recharged within a reasonable time to power the node during network joining while using a kinetic energy harvester. In that light, Kalita and Khatua [14] also enable a faster formation process with reduced energy consumption by proposing a channel condition-based dynamic beacon interval. Finally, Vilajosana et al. [15] proposed an energy consumption model for TSCH network. They calculate the average energy consumption and duty cycle, and discuss network configuration choices. However, both [14] and [15] do not evaluate the feasibility of energy harvesting.

As shown in Table I, we do not focus on one specific wireless technology or energy source, but present a feasibility analysis including different combinations of wireless technologies (LoRaWAN, BLE, and 6TiSCH) and energy sources (solar, kinetic, and RF) for IoT use cases. Moreover, our generic model is not restricted to the considered combinations but allows us to include any wireless technology and ambient energy source.

Several works do consider multiple wireless technologies in their feasibility analysis. Van Herbruggen et al. [16] investigated the possibility of using the vibrational energy at a horse's leg to power a perpetual monitoring device. Based on an existing model, they study the average delivered power for four natural gaits of the horse. The authors consider six wireless technologies (WiFi, BLE, ultra-wideband (UWB), LoRa, SigFox, and IEEE 802.15.4) in their feasibility analysis for which they derive the power consumption during transmission and various sleep states. Based on the average delivered power and power consumption, the achievable duty cycle of the device is calculated for each wireless technology when using a battery as a storage element. However, the leakage current of the battery, the medium access control (MAC) operation, and the time for switching between states are ignored. Yuksel and Fidan [17] developed an energy-aware system model to establish a batteryless operation of devices with multiple wireless technologies (Wi-Fi, Bluetooth, LoRa, SigFox, and LTE-M) and designed a solar-powered energy harvesting system. The system model includes a network model, IoT node model, energy harvesting model, energy storage model, and power management model. The authors consider an ideal supercapacitor, neglecting charge redistribution and leakage current. Through simulations, based on a probabilistic sensing model, they evaluate how the proposed method influences the energy efficiency of the network. Finally, Saavedra et al. [18] performed a feasibility analysis of different IoT wireless technologies (SigFox, LoRaWAN, NarrowBand IoT (NB-IoT), WiFi, and BLE) in combination with solar, RF, and magnetic induction energy for a smart metering use case. Based on experimental measurements, they analyze the power consumption of the wireless technologies as a function of data size, connection establishment, and transmission

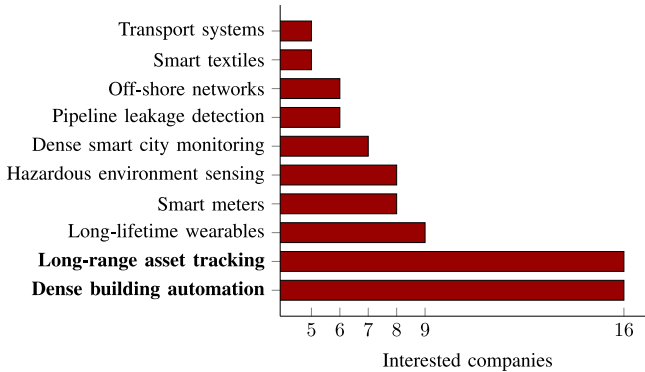


Fig. 1. Common IoT use cases eligible for energy harvesting. For each application, the number of interested companies, out of 21, is given. Based on the interest, long-range asset tracking and dense building automation were selected for the feasibility and tradeoff analysis.

time. They assess which combinations are feasible, by comparing the average power consumption to the average harvested power.

In contrast, we analyze the feasibility of energy harvesting from a different perspective than existing works. Instead of calculating the average power consumption or modeling the complete wireless technology operation, we consider the worst case scheduling scenario of the wireless technology from an energy harvesting perspective and include control traffic. As such, the intermittent nature of wireless IoT technologies and the behavior of the capacitor is taken into account. Furthermore, we assume a nonideal storage element by considering a realistic capacitor charging model, including leakage current, and considering the energy conversion efficiency.

III. ENERGY HARVESTING IN IOT

To gain insight into the needs and expectations of the industry regarding the use of energy harvesting in IoT, we present the results of a survey featuring 21 companies involved in IoT and interested in deploying energy harvesting solutions. The companies are located in Flanders, Belgium and are active in smart utilities, smart buildings, industry 4.0, logistics, and e-health. To capture a representative view, they were chosen based on different core activities, such as hardware design, IoT and private network operators, healthcare wearables, freight tracking systems, building and industrial valve monitoring, IoT service providers, groundworks, logistics, drink water providers, etc. These results allow us to identify promising IoT use cases, energy harvesting sources, and wireless technologies from an industry perspective.

Fig. 1 lists ten use cases for energy harvesting systems and shows the number of interested companies. As can be seen, dense building automation and long-range asset tracking are most relevant as sixteen out of 21 companies are interested. This is in line with current market trends: the applications with the largest share in the IoT energy harvesting market are expected to be building & home automation, industry 4.0, logistics, and consumer electronics in the near future [19], [20]. Therefore, we selected these use cases to be evaluated in the feasibility and tradeoff analysis presented in Section VII.

TABLE II
TYPICAL REQUIREMENTS FOR TWO IOT USE CASES, BASED ON LITERATURE REVIEWS [12], [21] AND SURVEY RESULTS

	Long-range asset tracking	Dense building automation
Latency	> 1 s	10 ms - 1 s
Transmission interval	15 min - 24 h	1 s - 24 h
Data size	4 - 40 B	20 - 200 B
Range	100 - 1000 m	10 - 200 m
Mobility	Mobile	Static
Location	outdoor / indoor	indoor

Table II lists typical requirements of these use cases based on the feedback from the involved companies and requirements found in scientific literature [12], [21]. Latency, transmission interval, data size, and range are considered since they have the most profound impact on the energy consumption of the IoT device. Additionally, mobility and location are also included as they can influence the choice of wireless technology and energy harvesting source, respectively.

Fig. 2 depicts the currently employed wireless technologies by the companies. A wide range of technologies is available, such as LoRa(WAN), BLE, IEEE 802.11-based technologies (e.g., Wi-Fi HaLow), NB-IoT, IEEE 802.15.4-based technologies (e.g., ZigBee, 6TiSCH, WirelessHART, and ISA100.11a), etc. [21], [22], [23]. Based on the survey results, BLE, LoRa(WAN), IEEE 802.11-based technologies, SigFox, and NB-IoT all prove to be popular among the involved companies. We have chosen BLE and LoRaWAN as suitable technologies for the feasibility and tradeoff analysis because of their popularity, their employment of industrial, scientific, and medical (ISM) frequency bands, and divergent communication capabilities. LoRaWAN aims to provide long-range communication over multiple kilometers using sub-GHz frequencies with a relatively high latency compared to BLE, which has a shorter range over a single hop, due to using 2.4-GHz frequencies, but can achieve greater distances with BLE Long Range or multihop BLE Mesh. Moreover, both technologies offer low-energy consumption configurations (i.e., LoRaWAN Class A and BLE Mesh LPN), making them particularly suitable for energy harvesting use cases. In terms of asset tracking, the market share of LoRaWAN is expected to grow due to the capability of handling a high device density, whereas the increasing integration of Bluetooth with IoT applications contributes to its own market growth [24]. Moreover, Bluetooth is also popular for building automation use cases, due to its short-range communication capabilities in commercial and industrial environments [25]. In addition, IPv6 over the TSCH mode of IEEE 802.15.4e (6TiSCH) is also considered in the feasibility and tradeoff analysis because of its high interest in the research community, fitness for industrial environments, and low energy consumption. Moreover, both sub-GHz and 2.4-GHz ISM bands can be used to deploy 6TiSCH, trading range for energy consumption. The details and operation of the chosen wireless technologies are discussed in Section VI.

Common sources of energy harvesting for IoT include solar, thermal, kinetic, and RF energy [19], [20], [26], [27]. Fig. 3 depicts the number of companies that are interested in using

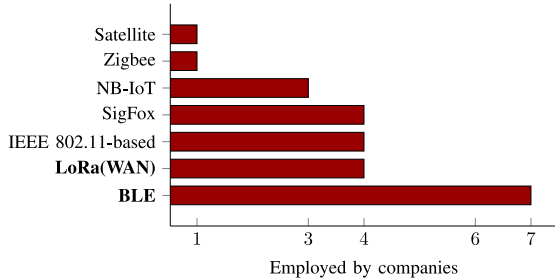


Fig. 2. Wireless technologies currently used by the involved companies. BLE and LoRaWAN were selected for the feasibility and tradeoff analysis.

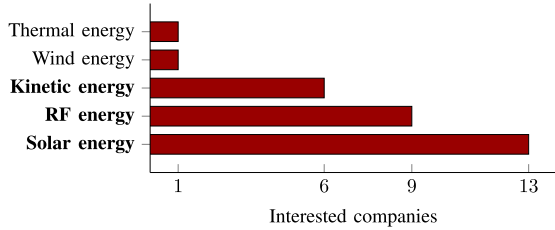


Fig. 3. Energy harvesting sources relevant for the involved companies. Kinetic, RF, and solar energy were selected as suitable harvesting sources for the feasibility and tradeoff analysis.

these sources for their IoT use cases. Due to their relevance for the industry, solar, RF, and kinetic energy are evaluated in the feasibility and tradeoff analysis as possible energy harvesting sources. For each source, two types of energy harvesting can be considered: 1) ambient and 2) intentional harvesting. The former uses ambient sources of energy (e.g., machine vibrations, RF signals from neighboring base stations, outdoor or indoor sunlight, etc.), and the latter harvests energy originating from an intentional event (e.g., movement of the device, wireless power transfer (WPT) or backscattering, intentional artificial light, etc.). Although intentional sources can be seen as a promising solution for powering IoT devices, they are not considered in the feasibility and tradeoff analysis due to their high degree of variability, making it hard to predict the available energy during a certain period. Ambient sources, however, also experience variability since the available energy highly depends on their environment (location, orientation, time of day, etc.). This unpredictability can be a severe drawback, especially in industrial settings with strict availability requirements. Nonetheless, the fact that they do not require the setup of dedicated external infrastructure (in contrast to, e.g., WPT) makes these energy sources very popular for energy harvesting. In Section V, some common values for ambient solar, kinetic, and RF energy harvesting sources are listed for different environments and scenarios.

Based on the results of the preliminary study, reflecting the needs and expectations of the industry, we have selected two relevant IoT use cases (long-range asset tracking and dense building automation), three suitable wireless technologies (LoRaWAN, BLE, and 6TiSCH), and three promising sources of ambient energy harvesting (solar, kinetic, and RF energy) to perform a feasibility and tradeoff analysis, presented in Section VII.

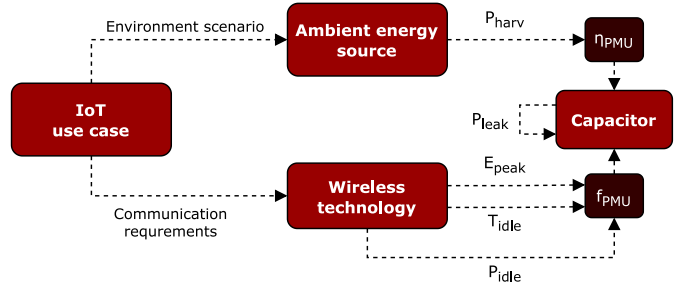


Fig. 4. Methodology for evaluating the feasibility of IoT use cases with energy harvesting. The required input and output for each building block can be provided by (a combination of) simulations, real-life experiments, mathematical models, machine learning, and technical specifications.

IV. WORST CASE ENERGY CONSUMPTION MODEL

This section describes the proposed model to analyze the feasibility of energy harvesting for IoT use cases. Fig. 4 depicts an overview of our model, which represents a typical energy harvesting system, including an energy source, wireless technology, supercapacitor, and PMU. In order to perform a fair comparison of the energy sources and wireless technologies, several assumptions for the different elements are defined. Then, we describe how to estimate the harvested power of the ambient energy source and the worst case energy consumption of the wireless technology, using the requirements and environment of the IoT use case. Based on the worst case energy consumption, the minimal required capacitance can be estimated. Finally, we calculate the charging time, using the harvested power and idle power consumption, while accounting for energy conversion losses by the PMU and leakage current of the supercapacitor. Comparing the recharge time with the required idle time allows analyzing the feasibility of the system.

A. Assumptions

To perform a fair comparison between different combinations of wireless technologies and ambient energy sources, and for simplicity, we define several assumptions.

A1: The storage element is a supercapacitor always operating between V_{\min} (turn-off voltage) and V_{\max} (maximum voltage). Therefore, for the system to be feasible, the load is never forced to turn off due to a lack of energy. However, the load can be turned off to limit energy consumption as part of the wireless technology operation. The supercapacitor experiences a leakage current I_{leak} , which is assumed to be constant over V_{\max} . As a result, the leakage power is $P_{\text{leak}} = I_{\text{leak}} \times V_{\max}$.

A2: A PMU takes care of the energy conversion between the energy source and supercapacitor, and between the supercapacitor and load. Therefore, we assume both the load and harvester operate at an equalized constant voltage V_{ref} . This also results in the operating range of the supercapacitor $[V_{\min}, V_{\max}]$ not depending on the operating range of the load, allowing for a fair comparison between devices. To account for energy conversion losses and the power consumption of the PMU, the PMU can be configured with variable

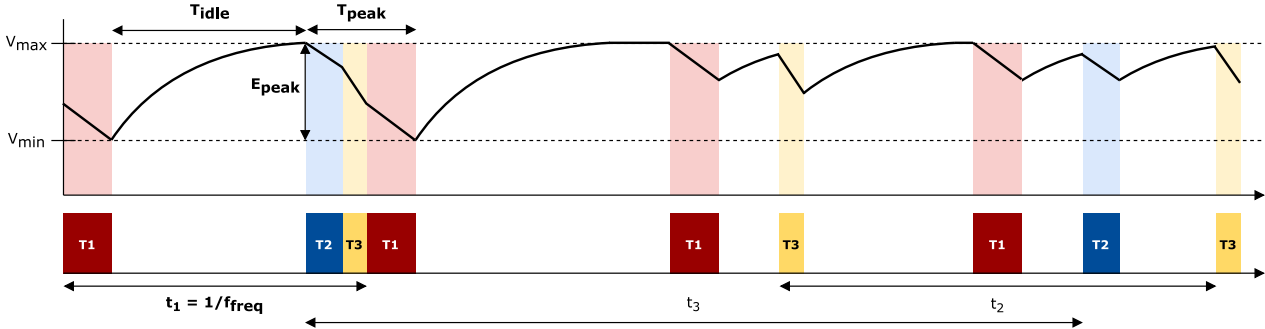


Fig. 5. Example of the worst case scheduling period of an energy harvesting device. The schedule includes three tasks and is depicted at the bottom, with the associated capacitor voltage at the top. The capacitor is charged during idle periods and discharged during the execution of tasks. T1 is selected as the *frequent task* and the *peak sequence* comprises the concatenation of all possible tasks, requiring the highest possible energy consumption and thereby imposing a minimal restriction of the capacitance. As the frequent task is scheduled at the end of the peak sequence, the *idle period* to recharge the capacitor is minimal. Therefore, this scenario is considered worst case since the capacitor needs to be fully recharged to its maximum value in a minimal amount of time.

efficiencies $\eta_{PMU,h}$ from the energy source to supercapacitor and $\eta_{PMU,l}$ from super capacitor to load, according to (1) and (2), respectively

$$P'_{\text{harv}} = \eta_{PMU,h} \times P_{\text{harv}} \quad (1)$$

$$P'_{\text{cons}} = \frac{P_{\text{cons}}}{\eta_{PMU,l}}. \quad (2)$$

A3: The energy harvesting node is part of a stable network, which implies the network joining process of the node is finished, nodes do not require to rejoin, and retransmissions are ignored. While the energy consumption is generally higher during initialization, this only constitutes a fraction of the operational lifetime of the device. Therefore, the joining process is ignored in the model, but Section VII-D describes the required extensions to include initialization, in addition to a motivation on why retransmissions can be ignored for the considered wireless technologies.

A4: We only consider uplink traffic from the energy harvesting node toward a network gateway, which is in line with most sensing applications. Including downlink traffic is seen as an extension to this model (Section VII-D). In addition, the latency is considered between the end of the sensing operation and the end of the sensor data reception by the network gateway. While further delays may be introduced by, e.g., the network backbone, such delays are not considered as they are implementation-specific.

B. Ambient Energy Source

The ambient energy source provides a continuous harvesting power P_{harv} , which is determined by the use case's environment. While a constant harvesting power generally does not reflect a realistic scenario, a practical variable harvesting power can be transformed into a constant one. The obvious choice is to average out the variable harvesting power over the considered time interval. However, smaller time intervals can be considered which requires a feasibility and tradeoff analysis for each time interval. Alternatively, the complete range or the bounds of the possible harvested power can be evaluated. For each energy source, we, therefore, define several environmental scenarios for which a fixed value or range of P_{harv} is

determined. In this work, the values of the available harvesting power, reflecting the various scenarios, are obtained through a literature review, as discussed in Section V. However, measurements or existing data sets for the targeted deployment location can also be used in case a more in-depth analysis is required.

C. Worst Case Wireless Technology Scheduling

Due to the nature of wireless IoT technologies and the characteristics of a supercapacitor, evaluating the average power consumption and the harvested power is not sufficient to analyze the feasibility of the system. After all, IoT devices reside most of their operational lifetime in an idle state, during which they consume little power, or are completely turned off. In contrast, the radio is the most power-hungry element of the IoT device, resulting in a current peak when activated. Therefore, long periods with low power consumption are alternated with short power peaks. Supercapacitors are able to deliver a high amount of power for a short time period, which is beneficial during short radio bursts. However, the energy density of a supercapacitor is much lower compared to that of a battery. As a result, the supercapacitor requires to be recharged during idle periods in order to deliver sufficient energy for the next radio burst.

Fig. 5 shows an example of a wireless sensor node's schedule at the bottom, where idle periods are alternated with three *tasks*, which we define as a sequence of operations that belong together and originate from a certain action. For example, a sensor reads a new value and transmits it to a server, which consequently replies with an acknowledgment. The reading of the sensor value, transmission to the server, and reception of the acknowledgment constitute a single task of the device. Tasks can be either periodical or event based, and their scheduling depends on the configuration of the wireless technology and the communication requirements of the use case. The top of Fig. 5 shows the associated voltage level of the capacitor, which is being recharged during idle periods and discharged during the execution of tasks. As described in A1, V_{\min} and V_{\max} represent the minimum and maximum voltage of the capacitor, respectively.

Instead of evaluating the feasibility of the energy harvesting system for the complete lifetime of the node during different periods, we identify the worst case scheduling period of the wireless technology. This simplifies the evaluation as only one period should be assessed: if the capacitor is able to handle this worst case period, all other periods are also feasible. The worst case scheduling period in Fig. 5 is shown at the beginning of the schedule. It starts with the execution of the *frequent task*, which is the task with the lowest interval t_1 . This can be the transmission/reception of a periodical control frame, a sense and transmit task, or any other frequently occurring task. At the end of the task, the capacitor is discharged to V_{\min} . The worst case scheduling period coincides ends with the highest possible energy consumption peak of the device, which is called the *peak sequence* and is represented by T_{peak} in Fig. 5. As can be seen, the peak sequence comprises all possible tasks of the wireless technology scheduled right after each other, thereby consuming the maximum amount of energy. Note that the frequent task is scheduled at the end of the peak sequence, which results in the shortest *idle period* T_{idle} in between the frequent task and the peak sequence.

This scheduling scenario is regarded as the worst case for an energy harvesting device for three reasons. First, T_{idle} has a minimal duration by scheduling the frequent task at the end of the peak sequence, hence limiting the allowed time to recharge the capacitor. Second, the peak sequence sets a lower bound on the capacitance as the capacitor should at least be able to store E_{peak} . This leads to a lower limit to recharge the capacitor, as a higher capacitance increases the recharge time. Finally, we assume the voltage over the capacitor is equal to V_{\min} at the beginning of T_{idle} , resulting in the maximal required energy that needs to be harvested within T_{idle} . While this worst case scenario might not occur frequently, the energy harvesting device should be able to cope with said scenario as it can possibly take place. Therefore, it suffices to only focus on this particular scenario to analyze the feasibility of the energy harvesting system. Additionally, only three parameters need to be extracted from the wireless technology in order to assess the feasibility: E_{peak} , T_{idle} , and P_{idle} . This makes the model generic as every wireless technology may be evaluated, provided these three parameters are known. In Section VI, we provide three examples of how to estimate these parameters for the selected wireless technologies, using existing measurements of off-the-shelf devices.

It must be noted that irrespective of the energy source and storage element, each wireless technology imposes limits on the achievable communication requirements of the use case. Therefore, before analyzing the feasibility of the energy harvesting system, it is crucial to identify the boundaries of the communication requirements for which the wireless technology is feasible. Naturally, it makes sense to only evaluate the energy harvesting system between these boundaries. Section VI therefore also covers the estimation of the latency and transmission interval boundaries for each wireless technology, as a function of other wireless technology parameters.

D. Minimal Capacitance Estimation

As mentioned previously, the peak sequence sets a lower limit to the capacitor size, which should be able to supply enough energy to the load to perform the peak sequence. The remaining energy in a capacitor can be calculated by $E = (C * V^2 / 2)$, where V represents the current voltage level. As a realistic capacitor operates between two voltage levels, defined as V_{\min} and V_{\max} in A1, the total available energy of that capacitor can be approximated by [28]

$$E_{\text{stored}} \approx \frac{C}{2} (V_{\max}^2 - V_{\min}^2). \quad (3)$$

The required energy to perform the peak sequence, in absence of harvesting, is calculated in (4). The PMU efficiency is taken into account by $\eta_{\text{PMU},l}$ and the leaked energy during the execution of the task is equal to $P_{\text{leak}} T_{\text{peak}}$. This is according to A1 and A2, respectively

$$E_{\text{req}} = \frac{E_{\text{peak}}}{\eta_{\text{PMU},l}} + P_{\text{leak}} T_{\text{peak}}. \quad (4)$$

Combining (3) and (4), the minimal required capacitance C_{\min} to perform the peak sequence in the absence of energy harvesting, is calculated in (5). The capacitor is fully charged before the task and reaches its minimum voltage level V_{\min} when the task is completed. Therefore, the load is not required to turn off, as per A1

$$C_{\min} \approx \frac{2 \left(\frac{E_{\text{peak}}}{\eta_{\text{PMU},l}} + P_{\text{leak}} T_{\text{peak}} \right)}{V_{\max}^2 - V_{\min}^2}. \quad (5)$$

E. Recharge Time Calculation

To perform a feasibility and tradeoff analysis for the system in Fig. 4, the idle time and required time to charge the capacitor should be calculated. T_{idle} can be calculated using f_{freq} and T_{peak} , as shown in

$$T_{\text{idle}} = \frac{1}{f_{\text{freq}}} - T_{\text{peak}}. \quad (6)$$

To calculate T_{charge} , we make use of the capacitor model in [7], which builds on the model introduced in [5]. Instead of using a harvested and consumed current, we use P'_{harv} , calculated in (1), as harvesting power and P_{cons} , calculated in (7), as consumed power. By using (1) and (7), the capacitor leakage and PMU efficiencies are taken into account in (8)

$$P_{\text{cons}} = \frac{P_{\text{idle}}}{\eta_{\text{PMU},l}} + P_{\text{leak}} \quad (7)$$

$$T_{\text{charge}} = -\frac{V_{\text{ref}}^2}{P_{\text{cons}}} C_{\min} \ln \left(\frac{V_{\max} - \frac{V_{\text{ref}} P'_{\text{harv}}}{P_{\text{cons}}}}{V_{\min} - \frac{V_{\text{ref}} P'_{\text{harv}}}{P_{\text{cons}}}} \right). \quad (8)$$

Using the above equations, the combination of energy source and wireless technology can be considered *feasible* if the idle time is sufficient to recharge the capacitor ($T_{\text{charge}} \leq T_{\text{idle}}$). In contrast, if $T_{\text{charge}} > T_{\text{idle}}$, the harvested power is not sufficient to recharge the capacitor in time. However, relaxing the communication requirements, wireless

TABLE III
HARVESTED SOLAR POWER (MPP) FOR AN INDOOR
AND OUTDOOR SOLAR PANEL OF 54 cm^2

Scenario	Illuminance/ irradiance	Indoor [29]	Outdoor [30]
Warehouse, coffee room	200 lx	0.289 mW	N.A.
	400 lx	~ 0.75 mW	N.A.
Regular office	600 lx	~ 1.24 mW	N.A.
	800 lx	~ 1.76 mW	N.A.
Mechanical workshop, office window	1000 lx	1.899 mW	N.A.
	1000 W/m ²	N.A.	240 mW
Clear sky	250 W/m ²	N.A.	54 mW

technology settings, or PMU configuration might increase T_{idle} . For that reason, although the combination is not feasible for the selected communication requirements and settings, it is labeled *plausible*. Finally, if the recharge time is negative, P_{harv} is insufficient compared to P_{cons} to charge the capacitor. Therefore, the selected combination is *infeasible*.

V. TYPICAL HARVESTED POWER FOR COMMON AMBIENT ENERGY SOURCES

This section includes some common values for the selected ambient energy sources, obtained from measurements, literature models, and technical reports. For each energy source, a range of possible DC power is given for multiple environmental scenarios. The considered energy harvesters and environmental scenarios for each energy source are chosen based on their relevance for dense building automation and long-range asset tracking use cases. However, other harvesters could be included for additional use cases and environments.

Table III lists the available maximum power point (MPP) for two off-the-shelf indoor and outdoor solar panels of 54 cm^2 , and for multiple indoor and outdoor environmental scenarios. Indoor environments include a warehouse or coffee room, a regular office, and a mechanical workshop or an office window. In outdoor scenarios, we consider a clear and cloudy sky. We used the PowerFilm Solar ©LL200-2.4-75 [29] and MPT4.8-75 [30] solar panels and obtained the MPP values from their technical documentation. However, as the technical documentation of the indoor solar panel only provides values for an illuminance of 200 and 1000lx, the intermediate values were obtained using an LTSpice model.¹

Although solar energy provides a high energy density and is considered a very promising energy source, not all environments experience sufficient light. Therefore, kinetic energy harvesters, of which piezoelectric, electrostatic, triboelectric, and electromagnetic transduction are the most commonly used types of harvesters, provide a suitable alternative. In this article, we consider piezoelectric harvesters because of their high energy density and easily tuned resonant frequency [31]. Table IV lists typical values of piezoelectric harvesters that may be deployed in industrial environments. A harvester connected to a vibrating machine with resonance frequency 50

¹Although Simulink-MATLAB would provide more accurate results, we intended to get an approximation of the values using free software. The values of the photovoltaic (PV) were deduced from measurements.

TABLE IV
HARVESTED KINETIC POWER FOR A VIBRATING MACHINE AND MOVING RAILWAY CAR

Scenario	DC power
Machine vibrations @50 Hz [31]	80–150 μW
Railway car @80 km/h [32]	100–250 mW

TABLE V
HARVESTED AMBIENT RF POWER FOR AN INDOOR AND OUTDOOR SCENARIO [33]

Scenario	Received power	Rectifier efficiency	DC power ²
LTE800 indoor	-5.80 dBm	~ 18 %	~ 50 μW
GSM900 indoor	-9.21 dBm	~ 9 %	~ 10 μW
LTE800 outdoor	-1.46 dBm	~ 27 %	~ 190 μW
GSM900 outdoor	-2.34 dBm	~ 26 %	~ 150 μW

Hz [31] and a moving railway car at 80 km/h [32] is considered. The available DC power equals 80–150 μW and 100–250 mW, respectively.

For ambient RF harvesting, we make use of the measurements carried out in [33]. The authors measured the received ambient RF power from 350 MHz to 16 GHz using an 410 cm^2 Archimedean spiral antenna in an indoor and outdoor scenario at the Universidad Politécnica de Madrid. LTE-800 and GSM-900 proved to be the most interesting frequency bands since they contained 82 % of the total power. Table V lists the received power for each frequency band and location. As the achievable DC power is not mentioned, we provide an estimate in Table V based on their measured rectifier efficiency at 870 MHz. The rectifier efficiencies are approximated based on [33, Fig. 15] and the DC power is calculated by multiplying the received power by the associated rectifier efficiency.

It should be noted that the values of Table V reflect an example scenario for a specific location and that the available ambient RF power is dependent on the deployment location. An overview of ambient RF energy densities across the world can be found in [34], in addition to measurements carried out in Montreal. Similarly, the values of Tables III and IV reflect example scenarios for our considered use cases but can be replaced by values for other use cases or environments.

VI. CHARACTERIZATION OF ENERGY PARAMETERS AND BOUNDARIES OF WIRELESS TECHNOLOGIES

The energy parameters of wireless technologies identified in Section IV allow for a generic model applicable to any wireless technology. However, the operation and scheduling of the technology need to be explored to obtain the values of these parameters. Nonetheless, measurements of an existing network deployment may also be used to acquire the energy parameters. In what follows, we calculate E_{peak} , T_{idle} , and P_{idle} as a function of parameters inherent to the selected wireless technologies (LoRaWAN, BLE Mesh, and 6TiSCH), using existing current consumption and time measurements of off-the-shelf

²Estimation based on the measured efficiency at 870MHz, exact values not mentioned in paper.

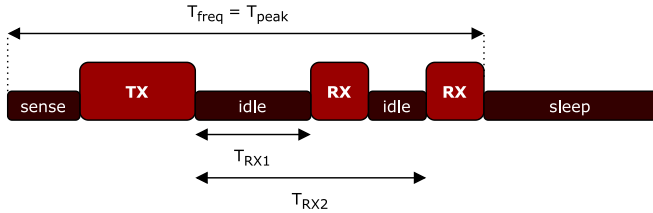


Fig. 6. LoRaWAN Class A scheduling. Since sense and transmit is the only task, it is considered as the peak sequence and frequent task.

devices. In addition, we determine boundaries for the guaranteed latency and transmission interval based on the wireless technology parameters.

A. LoRaWAN Class A

As discussed in Section III, LoRaWAN provides long-range communication over multiple kilometers by using sub-GHz frequencies. LoRaWAN devices use the long range (LoRa) PHYSical layer (PHY) while the upper layers are defined in the LoRaWAN specification [35]. Depending on the functionality and energy consumption requirements, three classes of end devices can be chosen: LoRaWAN Class A, B, or C. As LoRaWAN Class A provides the lowest energy consumption, it is best suited for energy-harvesting applications and therefore we only consider this class. Fig. 6 depicts the scheduling of a LoRaWAN Class A device; after an optional sensing operation, the device transmits (sensor) data to a LoRaWAN Gateway and waits for T_{RX1} before listening for downlink data. If nothing was received, the device listens a second time at T_{RX2} after the end of transmission. Subsequently, the device enters a sleep mode until the new uplink data is available. Because a LoRaWAN Class A device does not require any additional control traffic, only a single task can be defined, starting at the sensing operation and ending after the last reception window. As a result, this task can be considered as the frequent task and the peak sequence ($E_{\text{freq}} = E_{\text{peak}}$).

To calculate the energy consumption during the sense and transmit task, we make use of the current consumption and time measurements carried out in [7] for a LoRaWAN Class A device on a SODAQ ExpLoRer board, listed in Table VI. The measurements were performed at a voltage $V_{\text{ref}} = 2.7$ V, assuming a TX power of 14 dBm and only uplink traffic (A4). Instead of using a fixed payload (8 B) and LoRaWAN configuration, we consider these to be configurable. This way, the communication requirements of multiple IoT use cases can be evaluated. The number of transmitted symbols for a given payload and LoRaWAN configuration is calculated according to the LoRaWAN specification [35] in (9), where n_{pr} represents the number of preamble symbols, PL the payload in bytes, SF the spreading factor (SF), and CR the coding rate. Furthermore, IH determines if an explicit header is disabled and DE if the low data rate optimization is enabled. The SF determines the amount of spreading and can range from 7 to 12, where a higher SF results in a longer range and longer transmission time, with increased energy consumption and

TABLE VI
CURRENT CONSUMPTION AND TIME VALUES OF LORAWAN CLASS A DEVICE ON SODAQ EXPLORE BOARD [7]

State	Current consumption	Duration
Start-up	13 mA	13 s
TX	49.61 mA	T_{TX}
Idle 1	17.13 mA	0.92 s
RX 1	27.57 mA	0.09 s
Idle 2	17.12 mA	0.92 s
RX 2	27.73 mA	0.27 s
Idle 3	16.92 mA	1.18 s
Sleep	3.44 mA	T_{idle}
Off	0.0004 mA	T_{idle}

latency as a result

$$S_{\text{TX}} = n_{\text{pr}} + 4.25 + 8 + \max \left(\left\lceil \frac{8\text{PL} - 4\text{SF} + 44 - 20\text{IH}}{4(\text{SF} - 2\text{DE})} \right\rceil (\text{CR} + 4), 0 \right). \quad (9)$$

Using (9), the duration of a LoRaWAN transmission is given by (10), where BW indicates the bandwidth. However, depending on the chosen LoRaWAN configuration and the regional specification, a different maximum payload is specified, ranging from 11 to 222 B [35]. As a result, multiple frames might be required to transmit the complete data size

$$T_{\text{TX}} = S_{\text{TX}} \frac{2^{\text{SF}}}{\text{BW}}. \quad (10)$$

Notice that in Table VI, both a sleep and off state is given for T_{idle} . Therefore, one can choose to switch the device into sleep mode or turn the device off to save power. However, in case the device is powered off during T_{idle} , an additional start-up of 13 s is required. We calculate the energy consumption of a sense and transmit task in (11) using the values in Table VI, where E_{sense} represents the required energy to complete the sensing task, $E_{\text{start-up}}$ the required energy to start-up the radio (if any), and $T_{\text{TX},i}$ the duration of the i th frame out of N_f frames required to transmit the complete data size. $E_{\text{start-up}}$ equals 456 mJ for an off idle state and zero for a sleep idle state

$$E_{\text{peak}} = E_{\text{sense}} + E_{\text{start-up}} + \sum_{i=0}^{N_f-1} (166 \text{ mJ} + 134 \text{ mW} * T_{\text{TX},i}). \quad (11)$$

Similarly, T_{idle} is given in (12) [making use of (6)], where T_{sense} indicates the sensing time, T_{TI} the transmission interval, and $T_{\text{start-up}}$ the start-up duration (if any). The power consumption during these idle states are 9.29 mW and 1.08 μ W

$$T_{\text{idle}} = T_{\text{TI}} - T_{\text{start-up}} - \sum_{i=0}^{N_f-1} (2.2 \text{ s} + T_{\text{TX},i}) - T_{\text{sense}}. \quad (12)$$

Equation (12) immediately imposes a restriction on the transmission interval and latency. That is, the transmission interval may not be smaller than the peak sequence, which is simply the sense and transmit task in the case of LoRaWAN

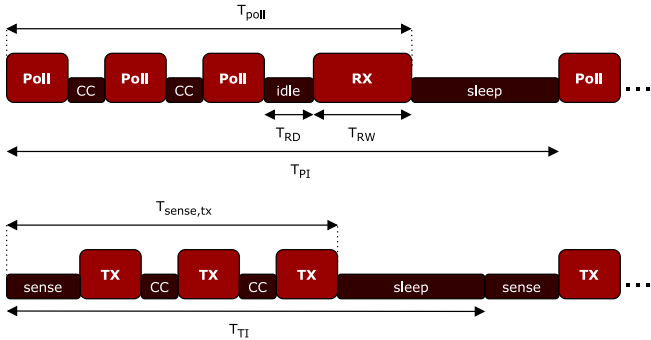


Fig. 7. BLE Mesh LPN scheduling. The top shows a periodic poll task with period T_{PI} to poll for any incoming downlink data. The bottom depicts a sense and transmit task, with a period equal to the transmission interval T_{TI} .

Class A. This lower bound is given in (13) and depends on the payload and LoRaWAN configuration [(10) and (9)]. The lower bound on the guaranteed latency is given in (14). Note that this is merely the guaranteed latency because of A3. In case interference would be considered resulting in possible retransmissions, no guaranteed latency can be identified and (14) provides a lower bound on the achievable latency. More on that in Section VI

$$T_{TI} \geq T_{start-up} + \sum_{i=0}^{N_f-1} (2.2 \text{ s} + T_{TX,i}) + T_{sense} \quad (13)$$

$$T_{lat} \geq T_{start-up} + \sum_{i=0}^{N_f-1} (2.2 \text{ s} + T_{TX,i}). \quad (14)$$

B. BLE Mesh Low-Power Node

Because of its low energy consumption, low cost, and support for mesh topologies, BLE has become an important wireless technology for IoT use cases. Compared to LoRaWAN, BLE has a shorter range but can extend this range over multiple hops by using BLE Mesh [36]. A BLE Mesh node can support four optional roles: relay, proxy, LPN, and friend node (FN). LPNs are nodes with a limited energy supply, making them suitable for energy harvesting use cases. An LPN is connected to a FN, which is part of the mesh network. To refrain LPNs from listening for incoming frames, the FN buffers incoming downlink frames.³ The LPN polls the FN periodically for buffered frames and enters a sleep or off state in between polls. In case the LPN wants to transmit an uplink frame, it can do so anytime to its FN. Therefore, polling for buffered frames and transmitting uplink frames (including a possible sensing operation) are considered two independent tasks.

Fig. 7 depicts the scheduling of a LPN for a poll task (top), and a sense and transmit task (bottom). The polling task starts with advertising a poll message on every advertising channel, requiring a channel change in between poll transmissions, portrayed as CC in Fig. 7. After the final poll message, the LPN

³Although we only consider uplink traffic, we also include the interaction with a FN to significantly reduce the amount of effort to extend the model with downlink traffic.

TABLE VII
CURRENT CONSUMPTION AND DURATION AT 1.8 V OF BLE MESH LPN DEVICE ON NORDIC NRF52840 BLE DEVKIT [10]

State	Current consumption	Duration
Wake-up TX	0.587 mA	2.940 ms
TX	9.09 mA	T_{TX}
CC	7.78 mA	0.029 ms
Radio off TX	6.60 mA	0.034 ms
Processing	2.17 mA	0.420 ms
Cool down	0.00653 mA	20.820 ms
Idle	0.00896 mA	T_{RD}
Wake-up RX	1.13 mA	1.910 ms
Listen	8.68 mA	T_{RW}
Radio off RX	4.69 mA	0.389 ms
Processing and cool down	0.00619 mA	23.410 ms
Sleep	0.00896 mA	T_{idle}

waits for a receive delay T_{RD} , before listening for any updates from its FN during receive window T_{RW} . Both durations can be configured up to a maximum of 255 ms. The polling interval T_{PI} is also configurable up to 96 h. In case the FN indicates it has buffered frames, the LPN may initiate a new polling task without having to wait for T_{PI} . Nonetheless, as per A4, we do not consider downlink traffic. The sense and transmit task is similar to the polling task, as the uplink frame is advertised on the three advertisement channels, with a channel change in between transmissions. However, the receive window is absent and an optional sensing operation precedes the first transmission.

The selection of the frequent task depends on the network configuration and the communication requirements. If $T_{PI} < T_{TI}$, the polling task is executed more frequently and is therefore selected as the frequent task. In contrast, sense and transmit becomes the frequent task if $T_{TI} < T_{PI}$. However, if both values are equal ($T_{TI} = T_{PI}$), the combination of both tasks is regarded as the frequent task. Regardless of the frequent task choice, the peak sequence contains both tasks.

The energy consumption calculations for each task are based on current consumption and time measurements performed in [10], listed in Table VII. The authors consider a BLE Mesh LPN implementation on a Nordic nRF52840 BLE devkit, using a reference voltage of $V_{ref} = 1.8$ V and TX power of 4 dBm. The top section of Table VII includes all states of a transmit task and the top and middle sections are the states of a poll task. Since no downlink traffic is considered, the radio is in listen state for the duration of the receive window T_{RW} . In order to determine the duration of a BLE transmission, Fig. 8 depicts the link layer frame structure for an advertising frame. The frame includes headers of an Advertisement Data structure, a nonconnectable and nonscantable protocol data unit (PDU), an Advertising PDU, and link layer headers and footer [36], which results in a total overhead of 18 B. As a result, the transmission time for a BLE advertising frame equals (15), where R equals the data rate, which can be either 1 or 2 Mbit/s. In contrast to LoRaWAN, we do not assume multiple transmissions because BLE offers a maximum payload of 251 B, which is above the considered data size range

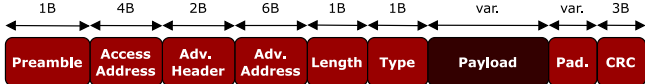


Fig. 8. BLE link layer frame structure for an advertising frame. The payload is appended with Advertisement Data structure, nonconnectable and nonscannable, advertising, and link-layer headers. The total header overhead equals 18 B.

of [4, 200 B] according to Table II

$$T_{TX} = \frac{8(PL + 18)}{R}. \quad (15)$$

The energy consumption of a sense and transmit task is calculated in (16), using the values in Table VII. Similarly, the energy consumption of a polling task is calculated in (17). $T_{TX,d}$ and $T_{TX,p}$ indicate the transmission time for a data frame and polling frame, respectively. Combining (16) and (17), results in a total peak energy consumption given in

$$E_{sense,tx} = E_{sense} + 6.2 \mu J + 16.4 \text{ mW} * 3T_{TX,d} \quad (16)$$

$$\begin{aligned} E_{poll} &= 28.2 \mu J + 16.4 \text{ mW} * 3T_{TX,p}, \\ &\quad + 16.1 \mu W * T_{RD} + 15.6 \text{ mW} * T_{RW} \end{aligned} \quad (17)$$

$$E_{peak} = E_{sense,tx} + E_{poll}. \quad (18)$$

The idle period in between the frequent task and the peak sequence is given by (19), using (6). Note that $1/freq$ depends on which task is most frequent. P_{idle} is calculated using the values in Table VII, and equals $16 \mu W$

$$\begin{aligned} T_{idle} &= \min(T_{TI}, T_{PI}) \\ &\quad - (74 \text{ ms} + T_{TX,p} + T_{TX,d} + T_{RD} + T_{RW}). \end{aligned} \quad (19)$$

The lower bounds on the transmission interval and guaranteed latency are specified in (20) and (21), respectively. The former is similar to (13), except that the advertisement frame is transmitted three times. As for the minimal guaranteed latency, this equals the time between the radio wake-up and the last transmission. If, however, the frame must be forwarded over multiple hops (N_{hops}), the latency increases with a transmission task for each hop. As with LoRaWAN, no guaranteed latency can be defined if interference from other nodes or networks is considered. In that case, (21) merely represents the minimal achievable latency

$$T_{TI} \geq 24.3 \text{ ms} + 3 * T_{TX} + T_{sense} \quad (20)$$

$$T_{lat} \geq T_{wake-up} + 3T_{TX} + 2T_{CC} + (N_{hops} - 1)T_{tx}. \quad (21)$$

C. 6TiSCH Leaf Node

6TiSCH was proposed by the Internet Engineering Task Force (IETF) 6TiSCH working group and offers a protocol stack to enable low-power IPv6 networks in industrial environments. It is based on the TSCH MAC mode of the IEEE 802.15.4-2015 standard [37] to offer reliable and energy efficient communication in the 2.4 GHz or sub-GHz ISM bands. A self-organizing, multihop network is established by the routing protocol for low-power and lossy networks (RPL) routing layer and IPv6 communication is enabled through an IPv6 over low-power wireless personal area networks (6LoWPAN)

adaptation layer. Additionally, the constrained application protocol (CoAP) provides a secure join process and RESTful interaction at the application layer. In what follows, we assume the reader has some knowledge about the operation of TSCH, RPL, and 6LoWPAN. For a detailed description of the 6TiSCH protocol stack, the reader is referred to [38] or to the individual technical documents of TSCH [37], RPL [39], and 6LoWPAN [40].

As the IEEE 802.15.4 standard does not define how to schedule timeslots and slotframes, we use the autonomous and decentralized Orchestra TSCH scheduler [41] because of its popularity and decentralized nature. More specifically, we opt for the lowest energy consumption received-based schedule (RBS), consisting of three slotframes: an EB slotframe (EBS), a receiver-based unicast slotframe (RBUS), and a broadcast slotframe (BS). In the EBS, each node is assigned one TX and one RX slot to transmit its own enhanced beacons (EBs) and listen for incoming EBs, respectively. An RBUS is used for unicast frames (i.e., data and destination advertisement object (DAO) frames), where a single RX slot and one TX slot for each neighbor are dedicated to each node. The BS includes a single shared slot during which nodes contend to transmit and listen for broadcast frames (i.e., a DODAG information object (DIO) frame). The size of the individual slotframes is configurable, where a smaller size increases the available rate of transmitted and received frames, but inevitably increases the average energy consumption as well. As a result, to limit energy consumption, slotframes should be chosen as long as possible, while still providing sufficient slots to transmit the required data or control traffic. This configuration results in an EBS duration similar to the EB period ($T_{EBS} \sim T_{EB}$) and a BS duration close to the DIO period divided by the number of neighbors ($T_{BS} \sim T_{DIO}/N_{nb}$). The duration of an RBUS (T_{RBUS}), however, depends on the communication requirements of the considered use case.

Fig. 9 depicts an example of an Orchestra RBS corresponding to the worst case scenario for an energy harvesting node. Red slots represent active slots and white slots idle slots. Note that idle RX slots are also regarded as active slots since the radio is activated for a short period of time to listen for incoming frames, resulting in nonnegligible energy consumption. Idle TX slots, however, are regarded as similar to nonactive slots because the radio is not activated. As shown in Fig. 9, the three slotframes repeat independently and nodes can only enter their idle state if none of the slotframes contain an active slot. Possible active slots include TX EB, RX EB, and RX idle for EBS, TX DIO, RX DIO, and RX idle for BS, and TX data, TX DAO, and RX idle for RBUS. RX data and RX DAO are not considered since we only assume uplink traffic (A4), and leaf nodes do not receive any DAOs.

To identify the tasks of a 6TiSCH leaf node, all slots are regarded as separate tasks except for a sense and TX task, which includes a sensing operation and TX data slot. The frequent task depends on the slotframe durations, the rate of control traffic, and data traffic rate. In a stable network, the EB interval will be the lowest of all control traffic. Therefore, either the EBS or RBUS will contain the most frequent task (slot). If the shortest slotframe contains slots with an equal

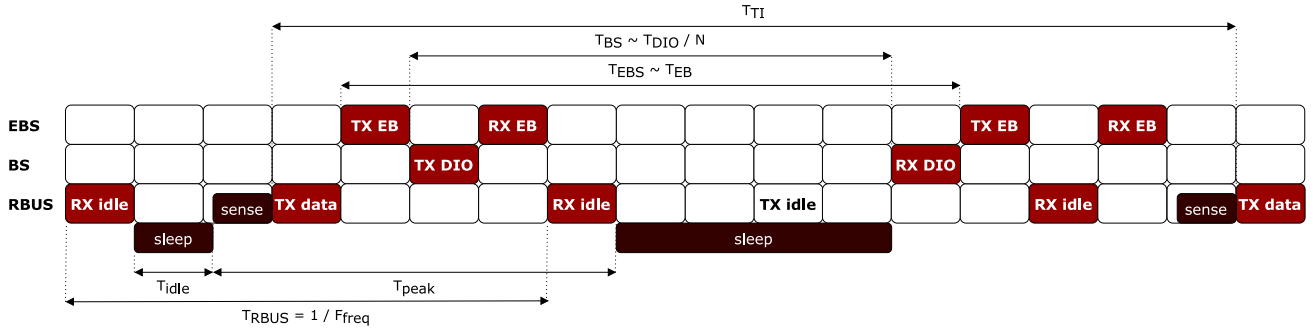


Fig. 9. 6TiSCH worst case scheduling using Orchestra Receiver-Based Schedule. Active slots are shown in red and idle slots are in white. The schedule includes an EB slotframe (top), a BS (middle), and RBUS (bottom). The node enters its idle state if all slotframes schedule an idle slot. The frequent task equals an RX idle frame and the peak sequence includes a sense and TX task, a TX EB, TX DIO, RX EB, and RX idle slot. Note that the sense and TX task may be replaced by a DAO TX slot in case the energy consumption of the latter is higher.

period, the slot with the highest energy consumption is chosen as the frequent task since it is consequently part of the peak sequence (at the end). As a result, if $T_{EBS} < T_{RBUS}$, the frequent task will be TX EB, since EBS ($\sim T_{eb}$) will be the shortest and TX EB is the slot with the highest energy consumption. Alternatively, if $T_{RBUS} < T_{EBS}$, either sense and TX data or RX idle will be selected as the frequent task. Which task will occur more frequently depends on the allowed network latency, because this directly impacts the size of T_{RBUS} (as explained later in this section). In the example of Fig. 9, T_{RBUS} is smaller than T_{EBS} , and the RX idle period is smaller than the sense and TX task period (equal to the transmission interval T_{TI}). Therefore, the RX idle slot is selected as the frequent task for this particular example. The peak sequence contains all possible tasks, i.e., a sense and TX data, TX EB, TX DIO, RX EB, and RX idle task. RX DIO is not included because it uses the same shared slot as TX DIO, but has a lower energy consumption (assuming the RX power consumption is lower than the TX power consumption, which is generally the case). Similarly, TX DAO uses the same slot as sense and TX data but is assumed to have a lower energy consumption ($E_{tx,DAO} < E_{sense,tx}$). If, however, $E_{tx,DAO} > E_{sense,tx}$, the TX DAO slot should be included instead.

The energy consumption calculations for each slot are based on current consumption and time measurements performed in [42] on a dual-band OpenMote device, using a 2.4-GHz CC2538 and 868-MHz CC1200 radio. The authors propose a model and performed measurements for multiple slot types, including a unicast TX and RX slot, a broadcast TX and RX slot, an idle TX and RX slot, and an idle slot. The current consumption and time values of a unicast TX slot for both radios are listed in Table VIII, where S_{TX} indicates the MAC protocol data unit (MPDU). The left column lists all the different radio states that make up a single unicast TX slot. Both radios use a data rate of 250 kbit/s resulting in a slot duration of 15 ms. Using the values of Table VIII, the energy consumption for a sense and TX task is calculated in (22) and (23) for the 2.4-GHz and 868-MHz radio, respectively

$$E_{sense,tx}^{CC2538} = E_{sense} + 336.5 \mu J + 0.174 \mu J * S_{TX} \quad (22)$$

TABLE VIII
CURRENT CONSUMPTION AND DURATION AT 3.3 V OF 6TiSCH DEVICE UNICAST TX SLOT ON OPENMOTE DUAL-BAND HARDWARE [42]

State	Duration [μs]		Current [mA]	
	CC2538	CC1200	CC2538	CC1200
Data offset start	105	105	13.97	15.06
Data offset	1515	1454	0.00156	0.270
Data prepare	60+ $0.875 * S_{TX}$	738+ $8.152 * S_{TX}$	13.97	17.49
Data ready	1954– $0.875 * S_{TX}$	1276– $8.152 * S_{TX}$	0.00156	2.64
Delay start	17	58	13.97	17.49
Data delay	349	369	27.55	50.24
Data start	16	16	31.47	54.26
TX data	$32 * (3 + S_{TX}) - 16$		27.55	50.24
ACK offset start	32	75	13.97	17.49
ACK offset	3769	3116	0.00156	2.64
ACK prepare	38	587	13.97	17.49
ACK ready	267	328	0.00156	2.64
ACK listen start	17	58	13.97	17.49
ACK listen	483	442	27.18	36.18
ACK start	16	15	26.94	50.63
RX ACK	880	881	23.16	46.73
TX process	225	619	13.97	15.06
Sleep	$5177 - 32 * S_{TX}$	$4783 - 32 * S_{TX}$	0.00156	2.64

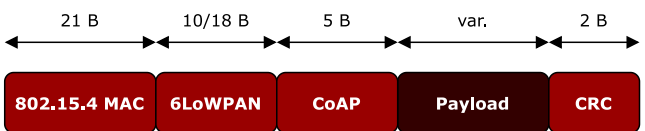


Fig. 10. 6TiSCH leaf node MPDU structure. The leaf node is part of a single PAN and RPL Instance and optional headers are elided. The total header overhead equals 38 B for a single-hop message and 46 B for a multihop message.

$$E_{sense,tx}^{CC1200} = E_{sense} + 682.1 \mu J + 1.873 \mu J * S_{TX}. \quad (23)$$

In order to determine S_{TX} , the MPDU structure of a 6TiSCH data uplink frame sent by a leaf node is depicted in Fig. 10. The frame includes an IEEE 802.15.4 MAC header and footer, a 6LoWPAN header, and a CoAP header. To limit header

overhead, we assume the leaf node is part of a single personal area network (PAN) and RPL Instance, and that optional headers are elided. In that case, the total header overhead equals 38 B for a single-hop message and 46 B for a multihop message, since for the latter an additional IPv6 destination address is included. Regarding the size of the control messages, we assume a fixed MPDU of 37 B for an EB and 96 B for a DIO and DAO. With these MPDU lengths, the values of Table VIII, and the measurements for the other slot types in [42], the energy consumption of the peak sequence is calculated in (24) and (25) for the 2.4-GHz and 868-MHz radio, respectively. In case $E_{tx,DAO} > E_{sense,tx}$, $E_{sense,tx}$ should be replaced with $E_{tx,DAO}$, which equals 45.9 μ J for the 2.4-GHz radio and 95.9 μ J for the 868-MHz radio

$$E_{peak,tx}^{CC2538} = 970.6 \mu\text{J} + E_{sense,tx}^{CC2538} \quad (24)$$

$$E_{peak,tx}^{CC1200} = 188.4 \mu\text{J} + E_{sense,tx}^{CC2538}. \quad (25)$$

The idle power consumption P_{idle} is calculated based on an idle slot with an energy consumption of 2.70 μ J (2.4 GHz) and 16.15 μ J (868 MHz). As the slot size is 15 ms, the idle power consumption equals 180 and 1076 μ W, respectively. The idle duration T_{idle} is given in (26), where T_{TS} equals the timeslot length, presuming the sensing operation is part of the peak sequence. Otherwise, T_{sense} should be left out of (26). Note that (26) depends on the relative size of T_{EBUS} and T_{RBUS} : the slotframe with the smallest size will determine the frequent task and, as a result, the idle duration

$$T_{idle} = \min(T_{RBUS}, T_{EBUS}) - 4 \times T_{TS} - T_{sense}. \quad (26)$$

Because of the synchronized MAC, 6TiSCH provides a deterministic, guaranteed latency, irrespective of A3. The lower and upper bounds of the latency are specified in (27). The lower bound takes place when the TX slot of the sensing device occurs right after the sensing operation, following the TX slots of any consecutive hops. In the upper bound, the first term accounts for the worst possible scheduling of the device's TX slot, i.e., right before the sensing operation, whereas $(N_h - 1)T_{RBUS}$ assumes the TX slot of any consecutive hops is scheduled right before the TX slot of the previous hop. In the final term, N_f represents the number of required fragments to send a frame. An extra T_{RBUS} is required for each additional frame, for each hop. The upper bound can therefore be regarded as the guaranteed latency. The minimal achievable transmission interval is specified in (28) and equals T_{RBUS} multiplied by the number of fragments

$$T_{lat} \geq T_{TS} \times N_h$$

$$T_{lat} \leq (T_{RBUS} - T_{sense}) + (N_h - 1)T_{RBUS} + N_h(N_f - 1)T_{RBUS} \quad (27)$$

$$T_{TI} \geq N_f T_{RBUS}. \quad (28)$$

Note that, by examining (12)–(14), (19)–(21), and (26)–(28), the interval between two frequent tasks for a 6TiSCH leaf node ($[1/f_{freq}] = T_{RBUS}$) not only depends on the transmission interval T_{TI} , but also on the latency since the guaranteed latency is a function of T_{RBUS} . This contrasts LoRaWAN and BLE Mesh, where the interval between two frequent tasks is either equal to the transmission interval or

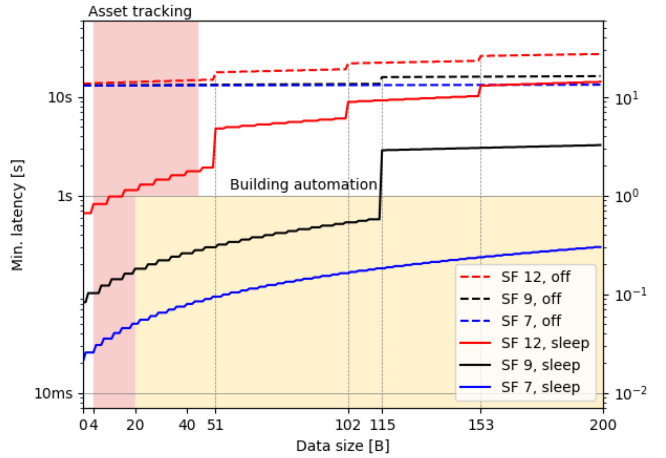


Fig. 11. Minimal achievable LoRaWAN Class A latency as a function of data size, SF, and idle state. The range of allowed latency and data size requirements (Table II) are highlighted in pink and yellow for long-range asset tracking and dense building automation, respectively. Blue, black and red lines correspond with SF 7, 9, and 12. Dotted lines represent the off idle state is used, whereas full lines indicate a sleep idle state.

to the period of a control frame. Therefore, the harvested power will determine both the latency and transmission interval of a feasible energy harvesting system, whereas, for LoRaWAN and BLE Mesh, only the transmission interval is affected.

VII. FEASIBILITY AND TRADEOFF ANALYSIS

Now that we have identified the harvested power of common ambient energy sources in Section V and characterized the energy parameters and boundaries of three widely used low-power wireless technologies in Section VI, we use our proposed model of Section IV to study the feasibility of energy harvesting for the use cases selected in Section III. To that end, the equations in Sections IV and VI were implemented in a Python script to determine the impact of network parameters, PMU configuration, and harvested power on the communication requirements, i.e., the required latency and transmission interval. The minimal (or guaranteed) latency is first evaluated for each wireless technology, using the lower bounds (or upper bounds) derived in Section VI. The resulting values are compared with the latency requirements for long-range asset tracking and building automation, presented in Table II, to assess which network configurations are feasible for each use case. Next, using a well-informed (set of) network configuration(s) following the latency evaluation, the minimal feasible transmission interval (for which $T_{idle} < T_{charge}$) is calculated as a function of the harvested power and PMU configuration. By comparing the feasible interval with the interval requirements of the selected use cases, and by comparing the associated feasible harvested power with the power values of ambient energy sources, it is possible to determine which energy sources are suited for which use case.

To establish a fair comparison between wireless technologies, we assume a fixed sensing operation of 10 ms and 50 mJ, a capacitor range of $V_{min} = 2.8$ V to $V_{max} = 4.5$ V, and a leakage current of 10 μ A. These values align with typical values for sensing operations [7], [9], an off-the-shelf PMUs [10], and existing supercapacitors [8], [9]. However, the parameters

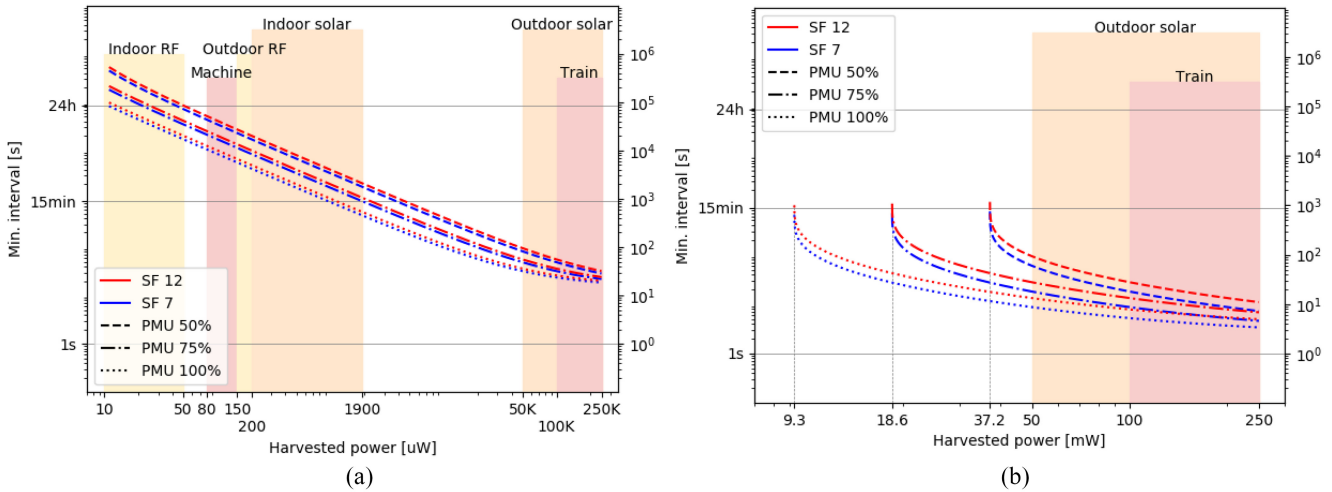


Fig. 12. Minimal feasible LoRaWAN Class A interval as a function of harvested power, SF, and PMU efficiencies for (a) off idle period and (b) sleep idle period. The available power range for solar, kinetic, and RF energy sources is highlighted in orange, pink, and yellow, respectively. Red lines indicate SF 12, blue lines SF 7, and different line types represent different PMU efficiencies.

can be easily altered in our Python script to evaluate other values.

A. LoRaWAN Class A

Fig. 11 depicts the minimal achievable latency (presuming A3) of a LoRaWAN Class A device versus the data size in bytes for the off idle state (dotted) and sleep idle state (full). Three different SFs are considered (7 in blue, 9 in black, and 12 in red) as the SF has the highest impact on the transmission time (and latency) and is directly related to the achievable range. In terms of the other LoRaWAN parameters, the preamble size equals 8, the bandwidth 125 kHz, code rate 0.8, there is a physical header present, but no low data rate optimization. Similar to the sensing, PMU, and leakage parameters, the values of the LoRaWAN parameters can be altered in our Python script. Fig. 11 also shows the allowed range in terms of data size and latency for long-range asset tracking in pink (4–40 B and >1 s) and for dense building automation in yellow (20–200 B and <10 ms–1 s), according to the typical requirements of Table II. Using the European regional specification in the 868-MHz ISM band, the maximum payload size of a LoRaWAN frame for SFs 7, 9, and 12 equals 211, 115, and 51 B, respectively [35].

As expected, the minimal latency increases with data size and SF, whereas the sudden jumps in latency for SF 12 at multiples of 51 B and for SF 9 at 112 B reflect multiple required transmissions ($N_f > 1$). Furthermore, the off idle state obligates a start-up period of 13 s, justifying the offset to the sleep idle state. As can be seen in Fig. 11, both idle states and all SFs are feasible for long-range asset tracking, merely since there is no upper bound (>1 s). If, however, 1 s is selected as upper bound, only the sleep idle state provides an adequate minimal latency. SF 7 and 9 can be used for all data sizes, whereas the data size of SF 12 is limited to 15 B. The 1 s upper bound coincides with the highest latency

limit for dense building automation. Therefore, again only the sleep idle state results in a sufficient latency. However, only data sizes below 115 B are feasible with SF 9 due to multiple required transmissions, in contrast to SF 7, which is applicable for the complete data size range. Nevertheless, a SF 7 will do for most (if not all) dense building automation use cases since they do not require a long range. For the 10-ms lower limit on the latency, none of the LoRaWAN configurations are suitable.

The minimal feasible interval for a LoRaWAN Class A device versus the harvested power, for SF 9 and 12 (blue and red, respectively), and PMU efficiencies of 50 %, 75 %, and 100 % (reflecting different line types), is depicted in Fig. 12. Fig. 12(a) represents an off idle period, whereas Fig. 12(b) indicates a sleep idle period. The data size was chosen to be 20 B, as this falls within the data size range of both use cases. Again, other data sizes could be evaluated, although the impact of data size on the feasible interval is minimal compared to the impact on the latency. This is also the case for the SF, as can be seen in Fig. 12. The PMU efficiency, however, does have a nonnegligible impact on the feasible interval. In the simulations of Fig. 12 we assumed both PMU efficiencies to be equal ($\eta_{PMU,h} = \eta_{PMU,l}$).

Fig. 12 also shows the range of available power for solar, kinetic, and RF energy sources (orange, pink, and yellow, respectively), and the typical required transmission interval for long-range asset tracking (15 min–24 h) and dense building automation (1 s–24 h). For long-range asset tracking, if the interval should be lower than 24 h, almost all ambient energy sources are feasible with the off idle period, except for indoor RF. In that case, either a high PMU efficiency is required or a high harvested power for indoor RF. However, if the interval needs to be below 15 min, only outdoor solar or the kinetic energy on a train is sufficient to power the energy harvesting system. Indoor solar energy might be possible, albeit a perfect PMU and high light availability is required. None of the

configurations for the off idle period are feasible given the 1-s interval restriction of dense building automation. Then again, the dense building automation requirements were already too strict in terms of latency for the off idle period (Fig. 11).

As shown in Fig. 12(b), a sleep idle period for LoRaWAN devices is feasible for outdoor solar and kinetic train energy sources ($P_{\text{harv}} \geq 9.3 \text{ mW}$), provided the minimal transmission interval is 15 min, which coincides with the minimum of long-range asset tracking. Therefore, both use cases are feasible for these energy sources, although the minimal 1-s restriction of dense building automation is not fulfilled.

B. BLE Mesh LPN

The minimal latency (assuming A3) for a BLE Mesh LPN is depicted in Fig. 13 as a function of data size, data rate (blue for 1 Mbit/s and red for 2 Mbit/s), and the number of hops to the network gateway (represented by different line types). The receive window T_{rw} and receive delay T_{rd} both equal their maximal value of 255 ms, but these values can be configured. Lowering these values would result in a shorter listening time, thereby reducing the peak energy consumption. As in Fig. 11, the range of communication requirements in terms of latency and data size are shown for both use cases. The latency increases with data size and decreases with data rate, although these parameters do not affect the latency as much as in LoRaWAN. This is mainly due to the cool-down state in Table VII, which takes 20.82 ms. In contrast, the time on air for transmitting three advertisement frames with a 200 B data size and the lowest data rate of 1 Mbit/s, equals 5.23 ms. However, the number of hops does have a large effect on the latency since the complete transmit task needs to be repeated (by another node, that is). If only a single hop is required (meaning the FN of the LPN is the network gateway), both strict and relaxed latency requirements of both use cases are satisfied. Both use cases will most likely require multiple hops, especially long-range asset tracking. However, the 1-s strict requirement for long-range asset tracking and relaxed for dense building automation are also fulfilled for two and three hops.

Fig. 14 shows the feasible transmission interval versus the harvested power, PMU efficiencies, and receive window/delay. For these calculations, the size of a polling frame is 37 B. As in Fig. 12, different PMU efficiencies are distinguished by different line types and the available power for the various energy sources is indicated, as are the transmission interval requirements for both use cases. The receive window is chosen equal to the receive delay, of which the blue lines represent 10 ms and red lines 255 ms. Other values could be equally well evaluated. For a feasible interval below 24 h, almost all energy sources are suitable ($P_{\text{harv}} \geq 17 \mu\text{W}$), except for indoor RF, which is only feasible for high PMU efficiencies and a high available indoor RF power. Below 15 min, representing the strict long-range asset tracking requirement, indoor/outdoor solar and kinetic train energy are adequate to power the device for all considered PMU efficiencies, except for very low indoor light levels and efficiencies of 50 %. If the PMU efficiencies are increased, outdoor RF and kinetic machine energy may

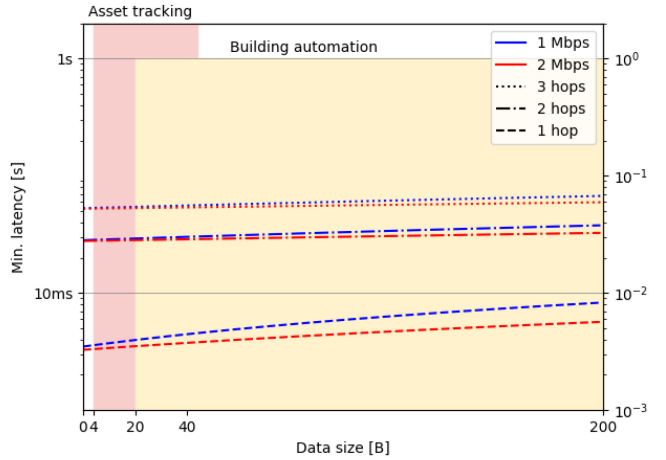


Fig. 13. Minimal achievable latency of a BLE Mesh LPN as a function of data size, data rate, and the number of hops. Blue and red lines correspond with 1 and 2 Mbit/s. The line type specifies the number of hops. Long-range asset tracking and dense building automation requirements are highlighted in pink and yellow, respectively (Table II).

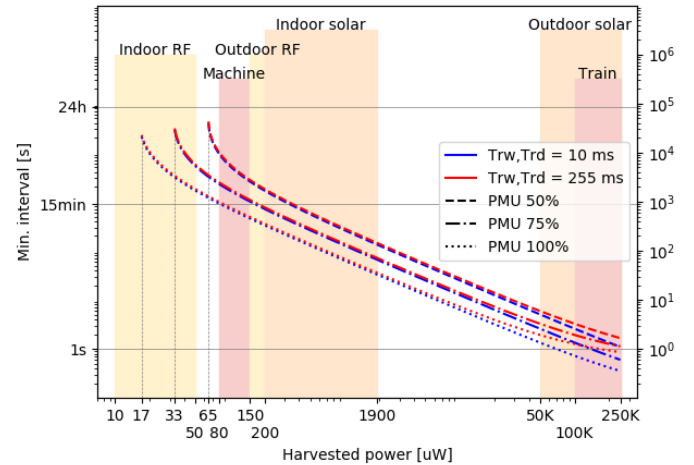


Fig. 14. Minimal feasible BLE Mesh LPN interval as a function of harvested power, receive window and delay, and PMU efficiencies. Blue lines indicate $T_{rw}, T_{rd} = 10 \text{ ms}$, red lines $T_{rw}, T_{rd} = 255 \text{ ms}$, and different line types represent different PMU efficiencies.

also be feasible. The 1-s strict requirement for dense building automation only seems feasible with a high PMU efficiency, a receive window/delay of 10 ms, and outdoor solar or kinetic train. However, these energy sources are not applicable to dense building automation use cases, in which devices are deployed mostly indoors.

C. 6TiSCH Leaf Node

As was discussed in Section VI, the guaranteed latency of 6TiSCH is also affected by the harvested power, in contrast to the minimal latency of LoRaWAN and BLE Mesh. Additionally, the lower bound on the feasible transmission interval (28) equals the guaranteed latency (27) for a single hop, aside from an offset T_{sense} . For that reason, Fig. 15 shows the guaranteed latency and minimum interval as a function of the harvested power, for the CC2538 2.4-GHz radio Fig. 15(a) and CC1200 868-MHz radio Fig. 15(b). For all

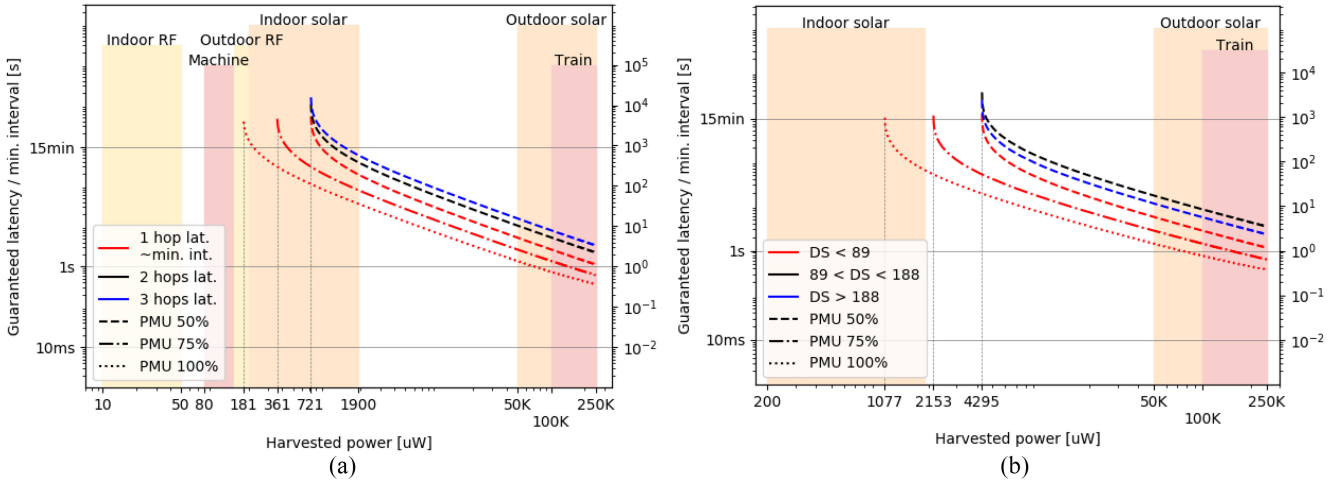


Fig. 15. Guaranteed latency and minimal feasible interval for a 6TiSCH node as a function of harvested power, number of hops, data size, and PMU efficiencies. (a) Impact of multiple hops for a CC2538 2.4-GHz radio and (b) impact of data size for a CC1200 868-MHz radio. The guaranteed latency for a single hop and the minimal interval are shown on the same lines as they are approximately equal.

simulations, $T_{eb} = 16$ s, $T_{DIO} = 16$ min, and $T_{DAO} = 15$ min, which coincide with commonly used values for a typical 6TiSCH network. For the CC2538 radio, the impact of the number of hops is shown, as this radio will most likely require multiple hops because of the 2.4-GHz frequency. Red lines indicate the single hop guaranteed latency, as well as an approximation of the minimal interval (ignoring the T_{sense} offset). Blue and black lines reflect two and three hops, respectively. The impact of the PMU efficiencies is also shown, although multiple hops are only considered for efficiencies of 50% to accommodate a clear graph. A latency below 1 s is feasible only for high power values of an outdoor solar and kinetic train, and for high PMU efficiencies. The strict latency requirement of dense building automation (10 ms) is feasible for none of the configurations, which makes sense as the timeslot duration is 15 ms. Therefore, in terms of latency, 6TiSCH only seems feasible for the long-range asset tracking use case. The strict interval requirement of 15 min can also be achieved for outdoor solar, trains, and indoor solar, albeit for the latter energy source this depends on the available light and the network/PMU configuration ($P_{\text{harv}} \geq 180 \mu\text{W}$). Long-range asset tracking use cases can therefore be regarded as feasible for outdoor solar, trains, and potentially indoor solar. Note that increasing the transmission interval any further does not result in a significant reduction of the required harvested power, because the harvested power at a 15 min interval is close to its feasibility limit. That is, P_{idle} equals 180 μW and P_{harv} should at least be higher than P_{idle} .

While the impact of the number of hops is shown for the CC2538 radio in Fig. 15(a), Fig. 15(b) shows the effect of the data size for the CC1200 radio. These calculations assume a single hop, such that the guaranteed latency approximately equals the minimal interval. Since the 6TiSCH overhead is 38 B and the maximum transmission unit (MTU) 127 B, a data size below 79 B results in $N_f = 1$, between 79 and 168 B in $N_f = 2$, and data sizes higher than 168 B require three fragments. Comparing Fig. 15(a) and (b), the number of required fragments has a similar impact to the number

of hops, which is logical when studying (27). Whereas the CC2538 radio was potentially feasible with indoor solar energy for long-range asset tracking use cases, the use of a CC1200 radio does not seem feasible, except for a perfect PMU and a very high light intensity ($P_{\text{harv}} \geq 1077 \mu\text{W}$). However, outdoor solar and trains remain feasible, irrespective of the employed radio.

D. Extensions Toward Other Use Cases

Although we cover a large combination of important technologies, use cases, and energy sources, other combinations could also be explored. However, the total number of combinations increases exponentially when adding other technologies, use cases, and energy sources. Nonetheless, our approach can be easily extended, mainly because of the limited amount of required parameters. Therefore, we list several possible extensions to our open-source model and feasibility and trade-off analysis, including our vision on how to include said extensions.

1) Network (Re-)Joining and Retransmissions: For the considered wireless technologies, we assume a stable network without taking the (re-)joining process and retransmissions into account, according to A3. For LoRaWAN Class A and BLE Mesh LPN devices, the joining process involves a couple of message exchanges between the device and the gateway/FN. However, the joining process of 6TiSCH networks requires a substantial number of energy and message exchanges, as highlighted in [13] and [14]. Nonetheless, the joining process is only a small part of the device's operational lifetime. For this reason, we propose treating the joining process separately from the stable operation, which we have included in our model. To achieve this, we suggest two recommendations for joining the network. First, the network should be formed gradually, allowing each node to join the network individually to spread out the network formation cost over a longer duration, and to reduce energy losses due to interference from other joining nodes. Once the network has stabilized, a new node is allowed

to join. Second, we propose using a separate energy storage element, such as a rechargeable battery or a larger supercapacitor, to supply sufficient energy for joining the network. In the case of a supercapacitor, the energy source charges it until the device can join the network, after which stable operation occurs with the minimal capacitor. By following these recommendations, energy harvesting nodes in 6TiSCH can join the network while our feasibility model remains valid during stable operation.

For some use cases, external factors such as variable electromagnetic properties of the environment and interference may affect the link quality. This might require nodes to change the network gateway or to retransmit frames. For a LoRaWAN Class A device, ACK requests are optional to reduce the energy consumption of the device. As a result, when disabled, LoRaWAN Class A devices will be ignorant of the channel conditions and continue to transmit uplink traffic to the gateway, without retransmissions. If ACK requests are enabled, (11)–(14) already include the effect of multiple transmissions, although a back-off is not considered. These equations could be extended with a back-off, but an evaluation is needed on the number of required retransmissions, given a certain network density. Therefore, in case of ACK requests, we propose to include a scalability analysis as part of the feasibility and tradeoff study, which is already covered in existing literature [43]. BLE Mesh LPNs neither expect ACKs and sufficient redundancy is foreseen by advertising frames on three different channels, which allows us to ignore retransmissions. For 6TiSCH, intranetwork interference is less of an issue due to the synchronized network protocol. This does not avoid interference from outside sources. However, TSCH uses channel hopping, which does help with avoiding interference. Furthermore, in case a retransmission should occur when using Orchestra, it would not be part of the peak sequence due to the combination of superframes. However, mobility in 6TiSCH networks would result in very high energy consumption since the number of control messages would skyrocket. Although some work has been done to establish mobility in 6TiSCH networks [44], this is inherent to the protocol design.

2) Downlink Traffic: As discussed in A4, we only consider uplink traffic in the feasibility and tradeoff study, as this is in line with most sensing applications. Especially when using energy harvesting, since the functionality of the devices needs to be kept minimal to reduce energy consumption. Nonetheless, the considered wireless technologies can be easily extended with downlink traffic, since the required MAC functionality is available: the LoRaWAN Class A schedule provides two reception slots, and the BLE Mesh LPN schedule also enables the reception of downlink traffic through the polling mechanism. Finally, 6TiSCH leaf nodes are able to receive frames during unicast RX slots. As a result, the only additional information that is required to include downlink traffic for these technologies is the timing and energy consumption of a downlink frame reception.

3) Additional Technologies, Energy Sources, and Use Cases: Finally, the feasibility and tradeoff study can be extended with additional technologies, energy sources, and use cases. Apart from LoRaWAN, BLE Mesh, and 6TiSCH,

other wireless technologies are suited for energy harvesting applications, such as NB-IoT, SigFox, ZigBee, etc. The characterization of the energy parameters and boundaries in Section VI for our selected technologies can be seen as an example for other technologies. By defining only three energy parameters, the threshold to include a wireless technology in the feasibility model is significantly reduced. A detailed knowledge of the wireless technology operation is not required to perform a quick feasibility analysis. After all, the peak energy consumption sequence, frequent task, and idle period can be equally well identified by analyzing the power consumption of an off-the-shelf device during a sufficiently long time interval. Alternatively, the energy parameters can also be collected by using high-end network simulators in the same manner. Furthermore, we only consider typical values of three common ambient energy sources, but other energy sources could be included as well. On top of technologies and energy sources, the feasibility and tradeoff analysis can be performed for other use cases, assuming different requirements than Table II. For example, the authors in [21] list requirements of other use cases.

VIII. CONCLUSION

In this article, we have presented a novel, generic model for analyzing the feasibility of energy harvesting for IoT use cases. The model uses a different approach compared to prior work. Existing models focus on calculating the average energy consumption of IoT devices, but these models do not capture the intermittent nature of wireless IoT use cases and technologies, and are hence not suitable to evaluate the capacitor's discharging behavior. Instead, our model focuses on periods with peak energy consumption and short idle times, as these pose the highest constraints on the capacitor recharging capability. We showed that the behavior of a wireless IoT device can be abstracted by a model with a limited number of well-chosen parameters that reflect such periods: frequent task interval, idle power consumption, and peak energy consumption. We applied this methodology to three common wireless technologies (LoRaWAN, BLE Mesh, and 6TiSCH) and were able to determine these parameters for different network configurations through power measurements of off-the-shelf devices and by making use of standard specifications. The abstraction to these parameters facilitates the inclusion of other wireless technologies as well since the parameters can be equally well determined by power analysis or by existing network simulators, without the need for detailed knowledge of the technology. Moreover, as the capacitor and PMU are fully configurable as well, we were able to show that efficiency has a significant impact on the achievable transmission interval.

Furthermore, we employed our model to analyze the feasibility in terms of latency and transmission interval of two prominent IoT use cases for energy harvesting: 1) long-range asset tracking and 2) dense building automation. LoRaWAN seems the most obvious choice for the former due to its long-range capabilities. Combined with outdoor solar or kinetic train energy, all requirements are fulfilled. A BLE Mesh LPN requires a lower harvested power but might need multiple

hops for long-range communication. Therefore, it is the best choice for dense building automation, although strict communication requirements will require a high harvested power. 6TiSCH could also be used, although the inherent control traffic poses restrictions on the achievable idle time between tasks. Moreover, an energy-intensive joining process and limited mobility may severely impact feasibility.

We hope this work can serve as an alternative method to analyze the feasibility of energy harvesting use cases and provides insights into which parameters are important when evaluating wireless technologies and energy sources. The model can aid researchers and developers in their design choices for perpetual IoT devices and compare combinations of wireless technology and energy sources.

REFERENCES

- [1] J. Hester and J. Sorber, "The future of sensing is batteryless, intermittent, and awesome," in *Proc. 15th ACM Conf. Embedded Netw. Sens. Syst.*, 2017, pp. 1–6. [Online]. Available: <https://doi.org/10.1145/3131672.3131699>
- [2] D. Van Leemput, "EH-feasibility." 2022. [Online]. Available: <https://github.com/imec-idlab/EH-feasibility.git>
- [3] H. H. R. Sherazi, M. A. Imran, G. Boggia, and L. A. Grieco, "Energy harvesting in LoRaWAN: A cost analysis for the industry 4.0," *IEEE Commun. Lett.*, vol. 22, no. 11, pp. 2358–2361, Nov. 2018.
- [4] M. Mabon, M. Gautier, B. Vrigneau, M. Le Gentil, and O. Berder, "The smaller the better: Designing solar energy harvesting sensor nodes for long-range monitoring," *Wireless Commun. Mobile Comput.*, vol. 2019, pp. 1–11, Jul. 2019.
- [5] C. Delgado, J. M. Sanz, and J. Famaey, "On the feasibility of batteryless LoRaWAN communications using energy harvesting," in *Proc. IEEE Global Commun. Conf. (GLOBECOM)*, Dec. 2019, pp. 1–6.
- [6] C. Delgado, J. M. Sanz, C. Blondia, and J. Famaey, "Batteryless LoRaWAN communications using energy harvesting: Modeling and characterization," *IEEE Internet Things J.*, vol. 8, no. 4, pp. 2694–2711, Feb. 2021.
- [7] A. Sabovic, C. Delgado, D. Subotic, B. Jooris, E. De Poorter, and J. Famaey, "Energy-aware sensing on battery-less LoRaWAN devices with energy harvesting," *Electronics*, vol. 9, no. 6, p. 904, 2020.
- [8] J. Finnegan, K. Niotaki, and S. Brown, "Exploring the boundaries of ambient RF energy harvesting with LoRaWAN," *IEEE Internet Things J.*, vol. 8, no. 7, pp. 5736–5743, Apr. 2021.
- [9] T. Sanislav, S. Zeadally, G. D. Mois, and S. C. Folea, "Wireless energy harvesting: Empirical results and practical considerations for Internet of Things," *J. Netw. Comput. Appl.*, vol. 121, pp. 149–158, Nov. 2018. [Online]. Available: <https://www.sciencedirect.com/science/article/pii/S1084804518302595>
- [10] A. K. Sultania, C. Delgado, C. Blondia, and J. Famaey, "Downlink performance modeling and evaluation of batteryless low power BLE node," *Sensors*, vol. 22, no. 8, p. 2841, 2022.
- [11] A. E. Xhafa, B. Campbell, and S. Hosur, "Towards a perpetual wireless sensor node," in *Proc. IEEE SENSORS*, Nov. 2013, pp. 1–4.
- [12] K. Das, P. Zand, and P. Havinga, "Industrial wireless monitoring with energy-harvesting devices," *IEEE Internet Comput.*, vol. 21, no. 1, pp. 12–20, Jan./Feb. 2017.
- [13] Z. J. Chew, T. Ruan, and M. Zhu, "Energy savvy network joining strategies for energy harvesting powered TSCH nodes," *IEEE Trans. Ind. Informat.*, vol. 17, no. 2, pp. 1505–1514, Feb. 2021.
- [14] A. Kalita and M. Khatua, "Channel condition based dynamic beacon interval for faster formation of 6TiSCH network," *IEEE Trans. Mobile Comput.*, vol. 20, no. 7, pp. 2326–2337, Jul. 2021.
- [15] X. Vilajosana, Q. Wang, F. Chraim, T. Watteyne, T. Chang, and K. S. J. Pister, "A realistic energy consumption model for TSCH networks," *IEEE Sensors J.*, vol. 14, no. 2, pp. 482–489, Feb. 2014.
- [16] B. Van Herbruggen, J. Fontaine, A. Eerdeken, M. Deruyck, W. Joseph, and E. De Poorter, "Feasibility of wireless horse monitoring using a kinetic energy harvester model," *Electronics*, vol. 9, no. 10, p. 1730, 2020. [Online]. Available: <https://www.mdpi.com/2079-9292/9/10/1730>
- [17] M. E. Yuksel and H. Fidan, "Energy-aware system design for batteryless LPWAN devices in IoT applications," *Ad Hoc Netw.*, vol. 122, Nov. 2021, Art. no. 102625. [Online]. Available: <https://www.sciencedirect.com/science/article/pii/S1570870521001517>
- [18] E. Saavedra, L. Mascaraque, G. Calderon, G. del Campo, and A. Santamaría, "The smart Meter challenge: Feasibility of autonomous indoor IoT devices depending on its energy harvesting source and IoT wireless technology," *Sensors*, vol. 21, no. 22, p. 7433, 2021. [Online]. Available: <https://www.mdpi.com/1424-8220/21/22/7433>
- [19] "Energy harvesting system market size, share & trends analysis report by technology (lights, vibration), by vibration technology (piezoelectric, electrostatic), by component, by application, and segment forecasts, 2020–2028." Grand View Research. 2021. [Online]. Available: <https://www.grandviewresearch.com/industry-analysis/energy-harvesting-systems-market>
- [20] M. Nikhil and P. Eswara, "Energy harvesting system by technology (light energy harvesting, vibration energy harvesting, radio frequency energy harvesting, and thermal energy harvesting), component (energy harvesting transducers, power management integrated circuits (PMIC), and storage system), and application (building & home automation, consumer electronics, industrial, transportation, and others): Global opportunity analysis and industry forecast, 2021–2030." Allied Market Research. 2021. [Online]. Available: <https://www.alliedmarketresearch.com/energy-harvesting-system-market-A13686>
- [21] A. Seferagić, J. Famaey, E. De Poorter, and J. Hoebeke, "Survey on wireless technology trade-offs for the industrial Internet of Things," *Sensors*, vol. 20, no. 2, p. 488, 2020. [Online]. Available: <https://www.mdpi.com/1424-8220/20/2/488>
- [22] L. Chettri and R. Bera, "A comprehensive survey on Internet of Things (IoT) toward 5G wireless systems," *IEEE Internet Things J.*, vol. 7, no. 1, pp. 16–32, Jan. 2020.
- [23] A. Nikoukar, S. Raza, A. Poole, M. Güneş, and B. Dezfooli, "Low-power wireless for the Internet of Things: Standards and applications," *IEEE Access*, vol. 6, pp. 67893–67926, 2018.
- [24] "IoT based asset tracking and monitoring market by connectivity (Wi-Fi, Bluetooth, cellular, NB-IoT, LoRa, SigFox, UWB, GNSS), application (automotive, manufacturing, & cold chain monitoring), region (North America, Europa, APAC, RoW)—Global forecast to 2027." Markets and Markets. 2022. [Online]. Available: <https://www.marketsandmarkets.com/Market-Reports/iot-based-asset-tracking-monitoring-market-118687881.html>
- [25] "Building automation system market by offering (facility management systems, security & access controls, fire protection systems, BEM software, BAS services), communication technology (wireless, wired), application and region—Global forecast to 2027." Markets and Markets. 2022. [Online]. Available: <https://www.marketsandmarkets.com/Market-Reports/building-automation-control-systems-market-408.html>
- [26] D. Ma, G. Lan, M. Hassan, W. Hu, and S. K. Das, "Sensing, computing, and communications for energy harvesting IoTs: A survey," *IEEE Commun. Surveys Tuts.*, vol. 22, no. 2, pp. 1222–1250, 2nd Quart., 2020.
- [27] M. M. Sandhu, S. Khalifa, R. Jurdak, and M. Portmann, "Task scheduling for energy-harvesting-based IoT: A survey and critical analysis," *IEEE Internet Things J.*, vol. 8, no. 18, pp. 13825–13848, Sep. 2021.
- [28] R. V. Prasad, S. Devasenapathy, V. S. Rao, and J. Vazifehdan, "Reincarnation in the ambiance: Devices and networks with energy harvesting," *IEEE Commun. Surveys Tuts.*, vol. 16, no. 1, pp. 195–213, 1st Quart., 2014.
- [29] S. Jones, 2 Cell 73 x 94 mm Tandem Low Light Module, PowerFilm Solar Inc., Ames, IA, USA, Feb. 2020. [Online]. Available: <https://www.powerfilmsolar.com/products/electronic-component-solar-panels/indoor-light-series/I2L200-2-4-75>
- [30] J. Fecht, 4 Cell 94 x 73 mm Tandem Module, PowerFilm Solar Inc., Ames, IA, USA, Jan. 2021. [Online]. Available: <https://www.powerfilmsolar.com/products/electronic-component-solar-panels/classic-application-series/mpt4-8-75>
- [31] I. Ahmad, L. M. Hee, A. M. Abdelrhman, S. A. Imam, and M. S. Leong, "Scopes, challenges and approaches of energy harvesting for wireless sensor nodes in machine condition monitoring systems: A review," *Measurement*, vol. 183, Oct. 2021, Art. no. 109856.
- [32] A. Hosseinkhani, D. Younesian, P. Eghbali, A. Moayedizadeh, and A. Fassih, "Sound and vibration energy harvesting for railway applications: A review on linear and nonlinear techniques," *Energy Rep.*, vol. 7, pp. 852–874, Nov. 2021.
- [33] A. Alex-Amor et al., "RF energy harvesting system based on an archimedean spiral antenna for low-power sensor applications," *Sensors*, vol. 19, no. 6, p. 1318, 2019.

- [34] X. Gu, L. Grawin, D. Douset, S. Hemour, and K. Wu, "Dynamic ambient RF energy density measurements of montreal for battery-free IoT sensor network planning," *IEEE Internet Things J.*, vol. 8, no. 17, pp. 13209–13221, Sep. 2021.
- [35] "LoRaWAN® 1.1 specification," LoRa Alliance Tech. Committee, Fremont, CA, USA, Rep., Oct. 2017. [Online]. Available: https://lora-alliance.org/resource_hub/lorawan-specification-v1-1
- [36] "Mesh profile Bluetooth specifications, v1.1," Bluetooth SIG, Kirkland, WA, USA, Rep., 2021. [Online]. Available: <https://www.bluetooth.com/specifications/specs/>
- [37] *IEEE Standard for Low-Rate Wireless Networks*, IEEE Standard 802.15.4-2015, Apr. 2016.
- [38] X. Vilajosana, T. Watteyne, T. Chang, M. Vučinić, S. Duquennoy, and P. Thubert, "IETF 6TiSCH: A tutorial," *IEEE Commun. Surveys Tuts.*, vol. 22, no. 1, pp. 595–615, 1st Quart., 2020.
- [39] T. Winter et al., "RPL: IPv6 routing protocol for low-power and lossy networks," IETF, RFC 6550, Mar. 2012. [Online]. Available: <http://www.rfc-editor.org/rfc/rfc6550.txt>
- [40] J. Hui and P. Thubert, "Compression format for IPv6 datagrams over IEEE 802.15.4-based networks," IETF, RFC 6282, Sep. 2011. [Online]. Available: <http://www.rfc-editor.org/rfc/rfc6282.txt>
- [41] S. Duquennoy, B. Al Nahas, O. Landsiedel, and T. Watteyne, "Orchestra: Robust mesh networks through autonomously scheduled TSCH," in *Proc. ACM Conf. Embedded Netw. Sens. Syst.*, Nov. 2015, pp. 337–350.
- [42] G. Daneels et al., "Accurate energy consumption modeling of IEEE 802.15.4e TSCH using dual-band OpenMote hardware," *Sensors*, vol. 18, no. 2, p. 437, 2018. [Online]. Available: <https://www.mdpi.com/1424-8220/18/2/437>
- [43] F. Van den Abeele, J. Haxhibeqiri, I. Moerman, and J. Hoebeke, "Scalability analysis of large-scale LoRaWAN networks in ns-3," *IEEE Internet Things J.*, vol. 4, no. 6, pp. 2186–2198, Dec. 2017.
- [44] B. Safaei et al., "Impacts of mobility models on RPL-based mobile IoT infrastructures: An evaluative comparison and survey," *IEEE Access*, vol. 8, pp. 167779–167829, 2020.



Dries Van Leemput received the B.Sc. degree, the first M.Sc. degree in electronics and ICT engineering technology, and the second M.Sc. degree in electrical engineering from Ghent University, Ghent, Belgium, in 2017, 2018, and 2020, respectively. He is currently pursuing the Ph.D. degree with the Internet Technology and Data Science Lab Research Group, Ghent University and imec, Ghent.

He joined the Internet Technology and Data Science Lab Research Group, Ghent University and imec. His research interests mainly revolve around multihop wireless sensor networks in industrial environments, Internet of Things, energy harvesting, network and energy modeling, and MAC protocol design for critical wireless systems.



Adnan Sabovic received the B.Sc. and M.Sc. degrees in telecommunications engineering from the Faculty of Traffic and Communications, University of Sarajevo, Sarajevo, Bosnia and Herzegovina, in 2016 and 2018, respectively. He is currently pursuing the Ph.D. degree with the University of Antwerp and imec, Antwerp, Belgium.

His research interests lie in the field of sustainable Internet of Things, energy-harvesting, low-power and batteryless communications, and energy optimization of IoT devices and their networks.



Khodr Hammoud (Graduate Student Member, IEEE) received the B.Sc. degree in electrical engineering and the M.Sc. degree in electrical engineering, specializing in electromagnetics from Eindhoven University of Technology (TU/e), Eindhoven, The Netherlands, in 2015 and 2017, respectively. He is currently pursuing the Ph.D. degree with the WaveCoRE Research Group, Electrical Engineering Department, KU Leuven, Heverlee, Belgium.

He joined the Livestock Business Unit, Nedap N.V., Groenlo, The Netherlands, as a Radiofrequency (RF) and Antenna Engineer in 2018. Since 2020, he has been working as an RF Engineer with the Identification Systems Business Unit, Nedap. He is focusing on sustainable IoT for indoor use through light energy harvesting. He is also interested in visible-light communications.



Jeroen Famaey (Senior Member, IEEE) received the M.Sc. degree in computer science and the Ph.D. degree in computer science engineering from Ghent University, Ghent, Belgium, in 2007 and 2012, respectively.

He is an Associate Professor with imec and the University of Antwerp, Antwerp, Belgium. He has coauthored over 150 articles published in international peer-reviewed journals and conference proceedings, and ten patent applications. His research focuses on performance modeling and optimization

of wireless connected systems, with a specific interest in sustainable IoT, and beyond-5G networks.



Sofie Pollin (Senior Member, IEEE) received the Ph.D. degree (Hons.) from KU Leuven, Leuven, Belgium, in 2006.

She continued her research on wireless communications, energy-efficient networks, cross-layer design, coexistence, and cognitive radio with the University of California at Berkeley, Berkeley, CA, USA, from 2006 to 2008. In 2008, she returned to IMEC, Leuven, to become a Principal Scientist with the Green Radio Team. She is currently an Associate Professor with the Electrical Engineering

Department, KU Leuven. Her research interests include networked systems that require ever more dense, heterogeneous, battery-powered, and spectrum-constrained networks.

Dr. Pollin is a BAEF Fellow and a Marie Curie Fellow.



Eli De Poorter received the master's degree in computer science engineering from Ghent University, Ghent, Belgium, in 2006, and the Ph.D. degree from the Department of Information Technology, Ghent University, in 2011.

He is currently a Professor with the IDLab Research Group, Ghent University and imec, Ghent, Belgium. He has over 200 publications in international journals or in the proceedings of international conferences. For his applied research, he collaborates with industry partners to transfer research

results to industrial applications, and to solve challenging industrial research problems. He is also the Co-Founder of the Lopos spin-off company, which offers privacy-aware UWB wearables for safety and social distancing. His team performs research on wireless communication technologies, such as (indoor) localization solutions, wireless IoT solutions, and machine learning for wireless systems. He performs both fundamental and applied research. For his fundamental research, he is currently the Coordinator of several research projects, such as SBO, FWO, and GOA.